TECHNICAL MEMORANDUMS

NATIONAL ADVISORY COMMITTEE FOR AERONAUTICS
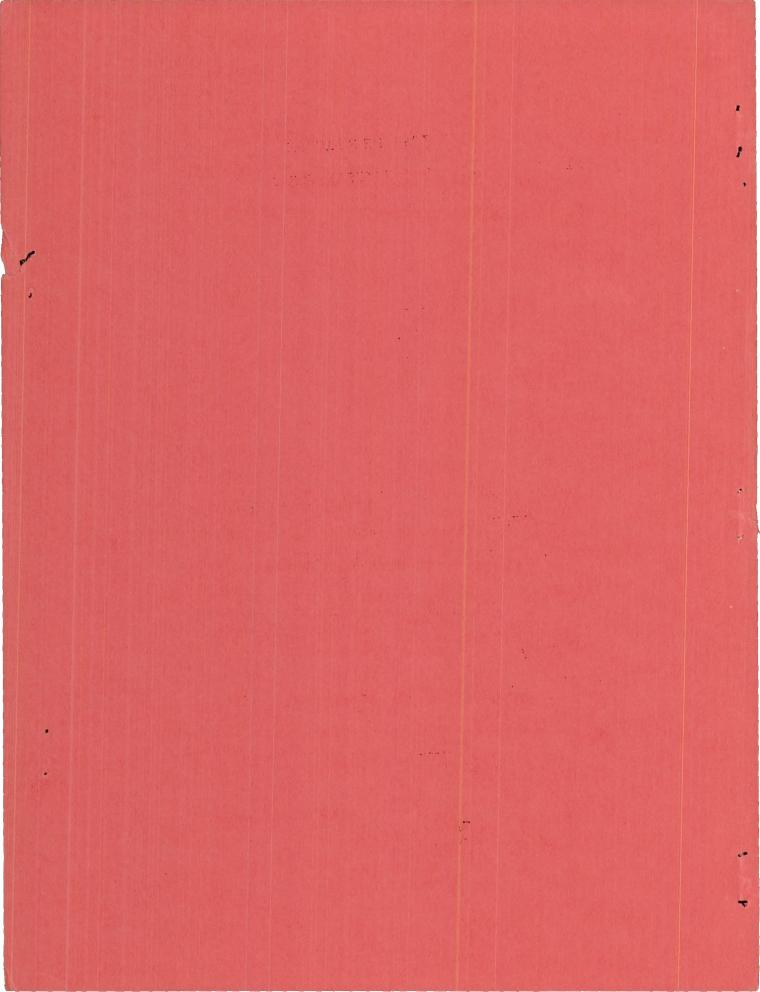
———

No. 935

———

APPLICATION OF THE METHODS OF GAS DYNAMICS TO

WATER FLOWS WITH FREE SURFACE

PART II.   FLOWS WITH MOMENTUM DISCONTINUITIES
(HYDRAULIC JUMPS)

By Ernst Preiswerk

Institut für Aerodynamik

Eidgenössische Technische Hochschule, Zürich

———

Washington
March 1940

NATIONAL ADVISORY COMMITTEE FOR AERONAUTICS

————

TECHNICAL MEMORANDUM NO. 935

————

APPLICATION OF THE METHODS OF GAS DYNAMICS TO

WATER FLOWS WITH FREE SURFACE*

PART II. FLOWS WITH MOMENTUM DISCONTINUITIES
(HYDRAULIC JUMPS)

By Ernst Preiswerk

SHOCK POLAR DIAGRAM

16. Introduction

It is known that in "shooting"** water under certain
conditions the velocity may strongly decrease for short
distances and the water depth suddenly increase. An un-
steady motion of this type is known as a hydraulic jump
(fig. 35). In this photograph the water flows from for-
ward to rear. In the forward part the water "shoots."
Over the entire width of the channel it jumps to a new
water level and flows with considerably less velocity in
the same direction toward the rear. The entire process
is practically stationary.

Hydraulic jumps occur only in shooting water; i.e.,
in water whose velocity of flow is greater than the wave
propagation velocity. In order to show this, let us im-
agine the forward water to be at rest and that from be-
hind there arrives the front of a water wave which arose
from the opening of a large sluice. If the wave were very
small it would move forward with the basic wave velocity
$\sqrt{gh_1}$. Since, however, it has finite height $h_2 - h_1$, it
moves to a first approximation with the velocity

——

** The term "shooting" has been used to denote the state
    of flow for which $c/\sqrt{gh} > 1$. (See T.M. No. 934.)

$$u_1 = \sqrt{g\,(h_1 + h_2)/2}\;\sqrt{(h_2/h_1)}\;{}^*$$

that is, more rapidly than $\sqrt{gh_1}$, and also than $\sqrt{gh_2}$. In this coordinate system, moving with the shooting water, the wave is not stationary. The water may now be considered as moving with the velocity u_1 with respect to the wave. The latter then remains at rest in space. The water ahead, however, is not at rest but has the flow velocity u_1, and this is greater than $\sqrt{gh_1}$. It has thus been shown that such hydraulic jumps can be stationary only in shooting water. If the wave existed in streaming water it would, on account of its propagation velocity, which in this case is larger than the flow velocity, travel upstream. There would be the usual outflow from upper to lower level without shock.** A shock (or hydraulic jump) in which the wave front is normal to the flow direction, is called a right hydraulic jump. It naturally has the property that the propagation velocity of the shock wave relative to the water is equal and opposite to the water velocity ahead of the jump.

More general than the right hydraulic jump, is the less familiar slant hydraulic jump (fig. 36). The water flows from left to right out of an open sluice. The water depth decreases and the velocity increases. The water flows from a constant upper water level into a basin with constant lower water level. Since the difference in head is greater than a third of the upper water depth, the water after escaping from the sluice receives, according to equation (42) a larger velocity than the basic wave propagation velocity, so that it shoots. It is thus possible that it accelerates so rapidly that the water surface of the flow becomes lower than the lower water level. There is a portion of the flow for which there is considerable pressure rise over a short distance. In this flow, however, the jump does not take place on a normal to the velocity but along a line oblique to the flow direction and we have a slant jump. On the meeting of the rear and forward jumps shown on the figure, there is a particularly strong pressure rise.

----

*This formula is obtained from a simple application of the continuity and momentum equations; for $h_a \longrightarrow h_1$, it naturally passes over into $u_1 = a_1 = \sqrt{g\,h_1}$. (See Lamb, reference 1, pp. 307-308.)

**The term "shock" will be used interchangeably with "hydraulic jump" and naturally has nothing to do with the compressibility of the water.

The slant jump, like the right, occurs only in shooting water. In order to be able to give a simple numerical treatment of the slant hydraulic jump, we make the assumption that the motion is entirely unsteady; i.e., that the water jumps suddenly along a line - the jump line - from the lower water level to the level after the jump. The simplest case of such a jump is obtained if a parallel flow is deflected by an angle β (fig. 37). The shock in the supersonic flow of a compressible gas has been treated in detail by Meyer and Busemann (reference 2). Here, however, it will appear that for the shock of the shooting water, the analogy with a compressible gas flow for $k = 2$, no longer strictly holds. The previous considerations involved as assumption the validity of the Bernoulli equation, which is equivalent to the assumption that the flow was without losses. With shock, however, kinetic energy is converted into heat. In a gas flow this again enters thermodynamically into the computation, whereas with the water flow it is to be treated as lost energy.

17. Shock Polars

For the case of the deflection of a parallel flow by the angle β, the jump line is a straight line through the corner, making an angle γ (fig. 37). For a very small deflection $\beta \longrightarrow 0$, the two following limiting cases are possible:

1. A right jump; γ is then a right angle.

2. The flow goes through undisturbed. This is the limiting case of a jump whose effect approaches zero. The jump line passes over into the Mach line through the corner, γ in this case being the Mach angle.

We shall take the x-axis such that it has the direction of the velocity of approach c_1. The components in the x and y directions are thus $u_1 = c_1$ and $v_1 = 0$. Let the water depth before the jump be h_1, the velocity after the jump c_2, its components in the x and y directions, u_2 and v_2. The water depth after the jump we shall denote by h_2; c_n and c_t, the components of the velocity normal and tangential, respectively, to the jump line. Here, too, we shall distinguish magnitudes before and after the jump by the subscripts 1 and 2, respectively. As control region for setting up the continuity and momen-

tum equation, we choose the region ABCDA (fig. 37).

With the above notation, the continuity equation reads:

$$h_1 \, c_{n_1} = h_2 \, c_{n_2} \qquad (71)$$

The momentum equation for the direction normal to the jump for the width AD = b, states that the decrease in outgoing momentum by that of the incoming momentum is equal to the force (area times pressure):

$$(\rho \, c_{n_2} h_2 b) \, c_{n_2} - (\rho \, c_{n_1} h_1 b) \, c_{n_1} = b h_1 \, g \rho h_1/2 - b h_2 \, g \rho h_2/2$$

or, rearranged:

$$h_1 \, c_{n_1}^2 + g \, h_1^2/2 = h_2 \, c_{n_2}^2 + g \, h_2^2/2 \qquad (72)$$

Writing finally the momentum equation for the direction tangential to the jump

$$(\rho \, c_{n_1} h_1 b) \, c_{t_1} = (\rho \, c_{n_2} h_2 b) \, c_{t_2}$$

there is obtained, taking account of the continuity equation (71):

$$c_{t_1} = c_{t_2} \qquad (73)$$

During the jump only the component of the velocity normal to the line is changed, the tangential component remaining unchanged.

As in the gas flow, it is convenient also for the treatment of the hydraulic jump, to pass from the field of flow to the velocity plane. Taking account of equation (73), there is obtained the diagram shown in figure 38. The region of the flow before the jump is in the velocity diagram represented by T. After the jump, P is the point of the hodograph corresponding to the flow. The jump itself is represented by the transition from T to P. The direction of the jump line in the flow is given in the hodograph by the normal to the segment TP, since this has the direction of c_t.

For a fixed velocity of approach, c_1, that is, for a

fixed point of the hodograph T, there are obtained for various deflection angles β, various end states, P. The totality of all end states which correspond to a fixed initial state, form a curve, the "shock polar" (fig. 38). If the initial state T is changed, then to each point T, there corresponds a shock polar. The entire family is the shock polar diagram (fig. 39). In the supplement, the latter is drawn for air on chart 3, and for water on chart 4.

The equation of the shock polars $v_2 = f(u_2)$ will now be determined. We start from the following five equations:

1. Continuity equation (71)

2. Momentum equation (72)

3. Energy equation*)

$$2g \, h_1 = 3 \, a_1^{*2} - u_1^2 \tag{74}$$

We also need the two geometrical relations:

$$4. \quad \frac{c_{n_1}}{c_{n_2}} = \frac{u_1 \, (u_1 - u_2)}{(u_1 - u_2) \, u_2 - v_2^2} {}^{**} \tag{75}$$

$$5. \quad c_{n_1}(c_{n_1} - c_{n_2}) = u_1(u_1 - u_2) {}^{***} \tag{76}$$

In the five equations referred to above, there occur the variables c_{n_1}, c_{n_2}, h_1, h_2, u_1, u_2, and v_2. Eliminating the first four, there is obtained the equation of the shock polar. (See equation (77).)

In order to carry out this elimination, we first substitute in equation (75) the continuity equation (71):

---

*) From the energy equation (9), we have:

$2g \, h_1 = 2g \, h_0 - c_1^2 = 2g \, h_0 - u_1^2$ (since $v_1 = 0$)

Substituting the critical velocity a^*_1 before the jump (equation (42)), we have:

$$2g \, h_1 = 3 \, a_1^{*2} - u_1^2 \tag{74}$$

(For footnotes ** and ***, see p. 6.)

$$\frac{h_2}{h_1} = \frac{u_1 (u_1 - u_2)}{(u_1 - u_2) u_2 - v_2^2} \tag{I}$$

Substituting the continuity equation (71) into the momentum equation (72), there is obtained:

$$h_1 c_{n_1}^2 + g h_1^2/2 = h_1 c_{n_1} c_{n_2} + g h_2^2/2$$

We thus have:

$$2g h_2^2 = 2g h_1^2 + 4 h_1 c_{n_1}(c_{n_1} - c_{n_2})$$

whence

$$\left(\frac{h_2}{h_1}\right)^2 = 1 + 4h_1 c_{n_1}(c_{n_1} - c_{n_2})/2gh_1^2 = \frac{2gh_1 + 4c_{n_1}(c_{n_1} - c_{n_2})}{2gh_1}$$

Substituting in the above the relations (74) and (76), we obtain:

(Footnotes from p. 5)

**From figure 38, we may read off directly the two equations:

$$u_2^2 + v_2^2 - c_t^2 = c_{n_2}^2$$

and

$$u_1^2 \qquad - c_t^2 = c_{n_1}^2$$

and their difference is:

$$u_1^2 - u_2^2 - v_2^2 = c_{n_1}^2 - c_{n_2}^2 \tag{a}$$

Similarly from figure 38, it may be seen that

$$(u_1 - u_2)^2 + v_2^2 = (c_{n_1} - c_{n_2})^2 \tag{b}$$

Dividing equation (a) by (b) and solving for the quotient c_{n_2}/c_{n_1}, we obtain the above relation (75). This relation must naturally exist since the three magnitudes u_1, u_2, and v_2, completely determine the figure 38.

***From figure 38, we read off directly,

$$c_{n_1}(c_{n_1} - c_{n_2}) = (u_1 \cos \epsilon)(c_{n_1} - c_{n_2}) =$$

$$= u_1 [\cos \epsilon.(c_{n_1} - c_{n_2})] = u_1 (u_1 - u_2) \tag{76}$$

$$(h_2/h_1)^2 = (3a_1^{*2} - u_1^2 + 4 u_1^2 - 4 u_1 u_2)/(3a_1^{*2} - u_1^2)$$

Only the positive root applies, since the water depths h_1 and h_2, and hence also their ratio, are naturally positive. We obtain:

$$\frac{h_2}{h_1} = + \sqrt{\frac{3a_1^{*2} - 4 u_1 u_2 + 3 u_1^2}{3a_1^{*2} - u_1^2}} \tag{II}$$

Setting finally the two right sides of equations (I) and (II) equal to each other (elimination of h_2/h_1) and solving the relation thus obtained for v_2^2, the required equation of the polars is finally obtained as

$$v_2^2 = [u_1 - u_2] \left[u_2 - u_1 \sqrt{(3a_1^{*2} - u_1^2)/(3a_1^{*2} - 4 u_1 u_2 + 3 u_1^2)} \right] \tag{77}$$

Substituting in the above $\bar{v}_2 = v_2/a^*_1$, $\bar{u}_2 = u_2/a^*_1$ and $u_1 = u_1/a^*_1$ as nondimensional velocities referred to a^*_1 the equation of the polars becomes:

$$\bar{v}_2^2 = [\bar{u}_1 - \bar{u}_2] \left[\bar{u}_2 - \bar{u}_1 \sqrt{(3 - \bar{u}_1^2)/(3 - 4 \bar{u}_1 \bar{u}_2 + 3 \bar{u}_1^2)} \right] \tag{77a}$$

These are the curves $f(\bar{u}_2, \bar{v}_2, \bar{u}_1) = 0$ with $\bar{u}_1$ as parameter drawn in figure 39 and on chart 4. They are similar to the shock polars of an ideal gas (chart 3), but show a characteristic difference. Whereas for the maximum velocity the shock polars in both cases become circles, the latter pass through the origin for water while for a gas, the origin is not attained.

In the case of a right jump, $v_2 = 0$. If we denote the velocity after the jump by u_{2g} (fig. 38), equation (77a) for the latter becomes:

$$0 = (\bar{u}_1 - \bar{u}_{2g}) \left((\bar{u}_{2g} - \bar{u}_1 \sqrt{(3 - \bar{u}_1^2)/(3 - 4\bar{u}_1 \bar{u}_{2g} + 3\bar{u}_1^2)} \right) \tag{a}$$

whence we obtain:

---

*From (a) there is obtained:

$\bar{u}_{2g} = \bar{u}_1 \sqrt{(3 - \bar{u}_1^2)/(3 - 4\bar{u}_1\bar{u}_{2g} + 3\bar{u}_1^2)}$. If this equation is squared, multiplied through by the denominator, and arranged, the resulting expression may again be divided by $(\bar{u}_1 - \bar{u}_{2g})$ and there is obtained a quadratic equation for $\bar{u}_1 \bar{u}_{2g}$ with the positive solution (77b).

$$\bar{u}_1 \, \bar{u}_{2g} = \frac{3 - \bar{u}_1^2}{8} \left[1 + \sqrt{1 + \frac{16 \, \bar{u}_1^2}{3 - \bar{u}_1^2}} \right] \qquad (77b)$$

The values computed from equation (77b) are collected in table IV. For an ideal gas the relation analogous to (77b) may be written in very elegant manner:

$$\bar{u}_1 \, \bar{u}_{2g} = 1 \quad (\text{Prandtl}) \qquad (77c)$$

Only for the case $\bar{u}_1 = 1$ does (77b) accurately agree with (77c).* Otherwise the right hydraulic jump leads to no simple relation like the normal shock of a gas. Within wide limits, however, equation (77c) may also be applied to water. (See values of $\bar{u}_1 \, \bar{u}_{2g}$ in table IV.)

We wish further to show that a very small jump has a jump line which in the limiting case is a Mach line. From the triangle TPU of figure 38,

$$\tan \gamma = (u_1 - u_2)/v_2$$

From the equation of the shock polars (77a), we have:

$$\left[\frac{\bar{u}_1 - \bar{u}_2}{\bar{v}_2} \right]^2 = \frac{\bar{u}_1 - \bar{u}_2}{\bar{u}_2 - \bar{u}_1 \sqrt{(3-\bar{u}_1^2)/(3-4\bar{u}_1\bar{u}_2+3\bar{u}_1^2)}} \qquad (77d)$$

A small jump is obtained if $\bar{u}_2 \longrightarrow \bar{u}_1$. The root in (77d) then approaches 1 and the entire expression becomes indeterminate. By differentiation of numerator and denominator with respect to the critical variable $\bar{u}_2$, there is obtained:

$$\left[\frac{\bar{u}_1 - \bar{u}_2}{\bar{v}_2} \right]^2_{\bar{u}_2=\bar{u}_1} = \frac{3 - \bar{u}_1^2}{3(\bar{u}_1^2 - 1)}$$

We then have:

$$(\sin^2 \gamma)_{\bar{u}_2=\bar{u}_1} = (\tan^2 \gamma)/(1 + \tan^2 \gamma) = (3-\bar{u}_1^2)/2 \, \bar{u}_1^2 \quad (a)$$

---

*For $\bar{u}_1 = 1$, the shock polar shrinks, however, into a point (fig. 39). The only possible state after the jump is thus $\bar{u}_{2g} = 1$. For this case we no longer have a finite jump but then the gas flow also agrees with the water flow.

On the other hand, for the Mach angle α

$$\sin^2 \alpha = (a_1/u_1)^2 \qquad (1)$$

For the wave velocity a_1, we have:

$$a_1^2 = g\, h_1 \qquad (2)$$

The energy equation (9) is

$$u_1^2 = 2g\, (h_0 - h_1) \qquad (3)$$

As reference velocity, we choose a_1^*. For this equation (42) applies

$$a_1^{*2} = \frac{2}{3}\, g\, h_0 \qquad (4)$$

Eliminating from equations (1) to (4) the magnitudes a_1, h_0, and h_1, there is obtained for the sine of the Mach angle α the relation

$$\sin^2 \alpha = (3 - \bar{u}_1^2)/2\bar{u}_1^2 \qquad (b)$$

Comparison of (a) and (b) then shows that

$$(\sin \gamma)_{u_2 = u_1} = \sin \alpha$$

18. Water Depths in Hydraulic Jump

Up to now we have investigated how the velocity changes in the case of a hydraulic jump. In this section we shall treat the water depths more in detail.

For a flow without jump, the energy equation (9) holds between c and h

$$c^2 = 2g\, (h_0 - h)$$

where the total head h_0 is a constant. In the case of a jump a portion of the kinetic energy of the water is converted into heat. For this reason the total head after the impact — which, to distinguish from h_0, we shall denote by h_0' — is smaller than it was before. For the flow after the jump, the relation between the velocity and the water depth is given by the energy equation in the following form:

$$c^2 = 2g \left(h_0{}' - h \right)$$

The new total head $h_0{}'$ is constant along a streamline but after the jump may vary from one streamline to another.

For gases (reference 2*), a clear picture of the pressures in the flow is obtained if the pressure is plotted as third coordinate over the velocity plane. For adiabatic flow there is thus obtained in the u,v,p space a surface of rotation whose meridian section represents p as a function of c:

$$c^2 = \frac{2k}{k-1} \frac{p_0}{\rho_0} \left[1 - \left(p/p_0 \right)^{(k-1)/k} \right] \qquad (3a)$$

For the two-dimensional flow of water with free surface, the magnitude h^2 corresponds to the pressure p in the gas flow. If we plot above the u,v plane, not the water depth but the values $t \equiv gh^2/2$, we shall find for the water in the u,v,t space the same relations that hold for a gas in the u,v,p space.

The representation in the $u,v,gh^2/2$ space is not very suitable for the practical computation of the jump. Nevertheless, we shall first learn the properties of this representation because it gives a very clear picture of the entire hydraulic jump process as regards the velocity and the water depth simultaneously.

In the flow of water without dissipation, the water depth h and hence $gh^2/2$, depends not on u and v individually, but only on the absolute value of the velocity $c = \sqrt{u^2 + v^2}$. Plotting t above the u,v plane, there is obtained a surface of rotation. Let us consider its meridian section $t = f(c)$ (fig. 40), abscissa c, ordinate t. From the Bernoulli equation (9), we have:

$$h = h_0 - c^2/2g \qquad (78)$$

whence

$$t \equiv gh^2/2 = (1/8g) c^4 - (h_0/2) c^2 + (gh_0{}^2/2) \qquad (79)$$

The characteristic shape of these curves of the fourth degree (fig. 40) which in our problem have a physical sense

_____
* Busemann, in Gasdynamik, pp. 374 and 439.

only from A to B, may easily be understood from figure
41, which shows the parabola (78) and its "square" (79).

For each total head h_0' there is one such curve.
The family of all these curves we shall denote as the t,c
diagram (fig. 42). As long as no jumps occur along a
streamline the relation between t and c, on account of
the constant total head, is given by a fixed curve of this
family. As soon as jumps occur along the streamline, the
t,c point on one curve "jumps" to another t,c curve.

Because the new total head for each jump becomes
smaller than the previous one, we come each time to a curve
lying closer to the origin and not the reverse.. To the
curves of constant total head h_0' = constant, which give
the relation between the $gh^2/2$ and c for the zero loss
flow, there correspond the adiabatics in the gas flow,
these being the lines of constant entropy, s = constant.
For the ideal gas, these are affine with respect to the
c axis but not for water.

The right hydraulic jump may very simply be studied
in the t,c diagram. Let us compute first the slope of
the tangent of the t,c curve to the axis of abscissas.
From equation (79),

$$\frac{dt}{dc} = \frac{c^3}{2g} - c \, h_0 = - c \, (h_0 - c^2/2g) \qquad (80)$$

and with the energy equation (78) this slope becomes

$$\frac{dt}{dc} = - c \, h \qquad (81)$$

We shall, furthermore, compute the intercept of the tan-
gent on the t axis, which is

$$QY = QP \tan \tau = c \, (c \, h) = c^2 \, h$$

On account of $t \equiv gh^2/2$:

$$OY = QY + OQ = h \, c^2 + gh^2/2 \qquad (82)$$

Physically both the slope of the tangent dt/dc and the
intercept of the tangent on the t axis have a meaning.
Through a vertical area in the flow normal to the stream-
lines and whose width is equal to the unit of length there
flows per unit time the volume c h. The magnitude $h \, c^2$

in equation (82) represents, except for a constant factor ρ, the momentum flowing through the same area per unit time, and the term $gh^2/2$ similarly, except for the constant factor ρ, represents the pressure force on this surface.

For the right hydraulic jump the continuity equation (71) is

$$h_1 c_1 = h_2 c_2 \qquad\qquad (71a)$$

The momentum equation (72) becomes:

$$h_1 c_1^2 + gh_1^2/2 = h_2 c_2^2 + gh_2^2/2 \qquad (72a)$$

These two equations, compared with (81) and (82) state the following:

1. From (71a) and (81): The tangent at the t,c curve at the point t_1,c_1 before the jump, has the same slope as the tangent at the point t_2,c_2 at the t,c curve after the jump.

2. From (72a) and (82): The t intercept of the tangent at t_1,c_1 is equal to the t intercept of the tangent at t_2,c_2.

Together they simply state that both tangents are one and the same straight line PQ (fig. 42). If the magnitudes t and c are given before the jump, the right hydraulic jump is represented in the t,c diagram by a jump from $P(t_1,c_1)$ on the tangent to the t,c curve through this point to $Q(t_2,c_2)$, where this tangent touches another t,c curve.

Since as a result of a jump, we arrive at a t,c curve which lies nearer the origin than the t,c curve before the jump, it may be seen from figure 42 that the hydraulic jump is possible only for points P before the jump which lie on the curve to the right of its point of inflection. This is precisely the case for shooting water since, according to (80),

$$d^2 t/dc^2 = 3c^2/2g - h_0$$

At the point of inflection this must be equal to zero, so that

$$c^2 = 2gh_0/3$$

This is the limiting velocity for streaming and shooting water.

Let us consider the slant jump. This may no longer be drawn in the t,c plane; we require the u,v,t space. Plotting the values $gh^2/2$ perpendicularly above the u,v plane, there is obtained for the case of a flow without losses the surface of rotation of a t,c curve. We shall denote such a surface as a "t-hill" (fig. 43). For each total head h_0', there is one such hill - each lying within the other. As long as no jumps occur in a flow, all possible corresponding values of u,v and $gh^2/2$ are, on account of the constant head h_0, given by a fixed t-hill. As soon as a jump occurs along a streamline, corresponding values of u,v and t jump to a new, smaller t-hill, which corresponds to the new total head h_0'. After the jump, however, the relation is again given by a fixed new t-hill.

Let $P(c_1,0,gh_1^2/2)$ denote the point in the u,v,t space before the jump; $Q(u_2,v_2,gh_2^2/2)$ after the jump (fig. 44). For the general slant jump there is obtained in the u,v,t space a clear representation similar to that for the right jump in the t,c diagram. This representation will include the right jump as a special case.

1. The slope of the tangential plane at the point P of the t-hill before the jump is, in the direction m_1, equal to zero, and in the direction r_1, equal to the slope of the meridian; i.e., equal to the slope of the t,c curve which, according to equation (81), has the value $c_1 h_1$. The slope of this tangent plane at the point P in the direction $\overline{PQ}$ thus becomes:*

$$\tan \sigma_1 = c_1 h_1 \cos \epsilon_1 = c_{n_1} h_1 \qquad (83)$$

The point Q lies on a t'-hill. The tangent plane has, in the direction m_2 the slope zero, and in the direction r_2, according to (81), the slope $h_2 c_2$. The slope of the tangent plane at the point Q of the t'-hill in the direction $\overline{PQ}$ is thus:

$$\tan \sigma_2 = c_2 h_2 \cos \epsilon_2 = c_{n_2} h_2 \qquad (84)$$

---

*The slope of a plane in any direction is equal to the slope of the plane in the direction of drop multiplied by the cosine of the angle between that direction and the corresponding direction.

Comparing (83) and (84) with the continuity equation for the slant jump (71), it is seen that the tangent plane at the t-hill at the point P before the jump in the direction $\overline{PQ}$ has the same slope as the tangent plane at the new hill at point Q after the jump in the same direction $\overline{PQ}$.

2.   Let us now compute the slope of the segment $\overline{PQ}$ in space to the u,v plane. The height of the point Q is $t_2 = gh_2^2/2$; that of P is t_1. The slope of PQ then becomes:

$$\tan \sigma_3 = (t_2 - t_1)/(c_{n_1} - c_{n_2})$$

Since, however, P and Q are the points before and after the jump, the continuity equation (71) and the momentum equation (72) are applicable. Substituting these two equations in $\tan \sigma_3$, there is obtained from (72):

$$t_2 - t_1 \equiv gh_2^2/2 - gh_1^2/2 = h_1 c_{n_1}^2 - h_2 c_{n_2}^2$$

and with (71) this becomes:

$$= h_1 c_{n_1}^2 - h_1 c_{n_1} c_{n_2} = h_1 c_{n_1} (c_{n_1} - c_{n_2})$$

Hence

$$\tan \sigma_3 = (t_2 - t_1)/(c_{n_1} - c_{n_2}) = h_1 c_{n_1} \qquad (85)$$

Comparison with the result found under 1 shows that the segment $\overline{PQ}$ has the same slope as the tangent plane at P and Q in the direction $\overline{PQ}$.

The segment $\overline{PQ}$ thus belongs to the two tangent planes and, as a common line of these two planes, has the property that it is tangent both to the t-hill and the t'-hill. This result would also have been found by determining the line of intersection of the two tangent planes at P (given by m_1 and r_1) and at Q (given by m_2 and r_2). There would then have been obtained the straight line $\overline{PQ}$ as the line of intersection.

The general hydraulic jump is thus represented in the u,v,t space as follows: Let P be a point before the jump. Drawing through this point an arbitrary tangent at the t-hill (the only restriction on the choice of this tangent is that it must pass within the t-hill), the point

indicating the state after the impact will be found where this tangent touches another t-hill of the family. To the degree of freedom of the tangent corresponds the degree of freedom of the deflection angle β . The projection on the u,v plane of all possible points of contact Q of the tangent of a fixed point P is the already computed "shock polar" through P.

The right hydraulic jump is obtained for a direction PQ with the angle $\epsilon_1 = 0$. Figure 42 simply shows the vertical section with $\epsilon_1 = 0$ through the t-hill family.

By the intensity of a jump we shall understand the ratio of the total head before the jump to the head after the jump, this ratio being a measure of the energy loss. The intensity is thus greater the more nearly the angle γ between the shock wave front and the initial direction approaches a right angle, since ϵ_1 then becomes smaller and the tangent PQ of the t-hill (total head h_0) at P touches t'-hills at Q (total head h_0') that lie more toward the interior. The right hydraulic jump has the maximum intensity.

It may be remarked further that the point Q of an arbitrary slant or right jump as the point of contact of a t'-hill is that point of the straight line PQ for which the new total head h_0' is a minimum. Each jump thus is such that the energy loss becomes a maximum. For the ideal gas, the surfaces corresponding to the t-hill are surfaces of constant entropy, and the shock is such that the increase in entropy is a maximum (Busemann).

The line joining all possible points of contact of the tangent at a fixed point P is the hydraulic-jump curve in the u,v,t space. It is a plane curve, its projection on the u,v plane being the already computed shock polar.

There is an entire family of shock curves in space (parameter point P). In their totality they form a certain surface. This we shall denote as the shock surface in the u,v,t space. For practical computation of the jump, the projections of the following three families of curves on the u,v plane are found convenient.

1. The curves of intersection of the shock surface with the tangent planes of all points $P(u,0,t)$; these give

the familiar shock polars (fig. 39).

2.   The curves of intersection of the shock surface with the planes parallel to the u,v plane; that is, contour curves. These are the lines of constant water depth h_2 (fig. 45 and chart 5).

3.   The curves of intersection of the shock surface with the family of t-hills. These give the lines of constant total depth after the jump; that is, lines of constant energy loss (fig. 46 and chart 4).

Lines h_2/h_0 = constant: From the five equations (71), (72), (74), (75), and (76) with the variables c_{n_1}, c_{n_2}, h_1, h_2, u_1, u_2, and v_2, there is obtained an equation of the form $F(u_2, v_2, h_2) = 0$ if the four magnitudes c_{n_1}, c_{n_2}, h_1, and u_1 are eliminated. These are the curves of constant water depth after the jump. In order to obtain these curves the elimination was partly carried out graphically. The method used will be briefly explained in what follows.

From (71) and (72) there is obtained:

$$gh_2^2/2 = gh_1^2/2 + h_1 c_{n_1} (c_{n_1} - c_{n_2})$$

which, with relation (76)

$$= gh_1^2/2 + h_1 u_1 (u_1 - u_2)$$

or

$$(h_2/h_0)^2 = (h_1/h_0)^2 + (4/3)(3/2gh_0)(h_1/h_0) u_1(u_1 - u_2)$$

Substituting the critical velocity equation (42): $a_1^{*2} = 2gh_0/3$) gives:

$$(h_2/h_0)^2 = (h_1/h_0)^2 + (4/3)\bar{u}_1(\bar{u}_1 - \bar{u}_2)(h_1/h_0) \qquad (86)$$

Solving for $\bar{u}_2$:

$$\bar{u}_2 = \bar{u}_1 - \left[(h_2/h_0)^2 - (h_1/h_0)^2 \right] / \left[\frac{4}{3} \bar{u}_1 (h_1/h_0) \right] \qquad (86a)$$

We still need equation (74), which reads:

$$2gh_1/3a_1^{*2} = 1 - \frac{1}{3}\bar{u}_1^2$$

Substituting (42) in the above there is obtained:

$$h_1/h_0 = 1 - \frac{1}{3} \bar{u}_1{}^2 \qquad (87)$$

In order to draw the lines h_2/h_0, two methods were employed:

a) Assume a fixed value $h_2/h_0 = k$ and various values $\bar{u}_1$ for the variable. To each $\bar{u}_1$ there corresponds by equation (87) a value h_1/h_0. With $\bar{u}_1$, the corresponding h_1/h_0 and the fixed h_2/h_0, there is obtained from (86a) the velocity component $\bar{u}_2$ after the jump. The point on the shock polar through $\bar{u}_1$ which has this abscissa $\bar{u}_2$, is a point of the curve $h_2/h_0 = k$. By varying $\bar{u}_1$ there is obtained the complete curve $h_2/h_0 = k$.

b) Determine the values h_2/h_0 along an arbitrary straight line in the u,v plane. (The straight line through $\bar{u} = 1$, $\bar{v} = 0$ was taken.) Assume $\bar{u}_1$; measure $\bar{u}$ at the point of intersection of the straight line with the shock polar for $\bar{u}_1$; substituting $\bar{u}_1$, the corresponding value h_1/h_0 obtained from equation (87) and the above determined value of $\bar{u}_2$ in equation (86) gives the value of h_2/h_0 at the point of intersection. By varying $\bar{u}_1$ there is obtained h_2/h_0 along the entire straight line. From these values there are obtained by interpolation points of the family of curves $h_2/h_0 = $ constant.

In particular, the values of h_2/h_0 may be computed for the right hydraulic jump. We have:

$$(h_2/h_0)^2 = (h_1/h_0)^2 + \frac{4}{3} (h_1/h_0) \bar{u}_1 (\bar{u}_1 - \bar{u}_{2g}) \qquad (86b)$$

Substituting in the above the values for $\bar{u}_{2g}$ computed from equation (77b), there are obtained the water-depth ratios h_2/h_0 given in table IV for the right hydraulic jump.

The maximum water depth in the state after the jump is obtained from equations (86b), (87), and (77b) for the jump which starts from the values $\bar{u}_1 = 3/\sqrt{5}$; that is, for $h_1/h_0 = 2/5$, $u_{2g} = 3/2 \sqrt{5}$, and is found to be $h_2/h_0 = 4/5$, and $h_0'/h_0 = 19/20$. We thus have the highest point of the above described shock surface in the u,v,t space.

19. Energy Loss During Hydraulic Jump

The energy loss during the jump bears a simple rela-
tion to the intensity of the jump - that is, to the two
total heads before and after the jump. In the flow over
a horizontal bottom the potential energy is a minimum if
the water depth h is zero. If we set the potential en-
ergy equal to zero, then for a mass of water m at a
depth h the potential energy is $P = mg\, h/2$.

Since the kinetic energy at points of rest is equal
to zero, the energy loss ΔE which occurs in the hydrau-
lic jump, may be computed as the difference of the poten-
tial energy at a point of rest before and after the jump.
For the mass of water m, this becomes:

$$\Delta E = mg\,(h_0/2 - h_0'/2)$$

Dividing by the energy before the jump, $E = mg\,\dfrac{h_0}{2}$, the
relative energy loss is obtained as

$$\Delta e = \Delta E/E = 1 - h_0'/h_0 \tag{88}$$

This is the relative energy converted into heat. For
water, it is to be considered as "lost." In a gas, how-
ever, where the heat content is the magnitude that corre-
sponds to the water depth, the total heat content remains
the same before and after the shock. For the gas, the
heat arising during the shock is not "lost" energy. The
energy equation is the same before and after the shock:
$c^2 = 2g\,(i_0' - i) = 2g\,(i_0 - i)$.

Now will be computed the curves of constant total
depth h_0' after the jump. We start from the Bernoulli
equation which for the flow after the jump reads:

$$c_2{}^2 = 2g(h_0' - h_2)$$

This equation divided by $a_1^{*2} = 2gh_0/3$, gives:

$$(c_2/a_1^*)^2 = 3\,(h_0'/h_0 - h_2/h_0) \tag{89a}$$

and solved for h_0'/h_0:

$$h_0'/h_0 = h_2/h_0 + \frac{1}{3}\,\bar{c}_2{}^{2\,*)} \tag{89b}$$

---

*) The values $\bar{c}_2,\ \bar{u}_2,\ \bar{v}_2$ are the velocities referred to a_1^*;
for example, $\bar{c}_2 = c_2/a_1^*,\quad \bar{u}_{2g} = u_{2g}/a_1^*$.

From the above formula the curves h_0'/h_0 = constant (fig. 46) were drawn similar to those for h_2/h_0 = constant. The following methods were employed:

1. The values h_0'/h_0 for the right hydraulic jump - that is, along the u-axis, $(v_2 = 0)$ - are obtained by substituting the previously computed values h_2/h_0 and u_{2g} ((77b), (86b), (87)) in equation (89b). They are also given in table IV.

2. Along the circle, $h_2/h_0 = 0$ $\bar{c}_2$ may be read off directly, and from equation (89b), $h_0'/h_0 = \frac{1}{3} \bar{c}_2^2$.

3. Along general arbitrary curves - in particular, along circles about the origin ($\bar{c}_2$ = constant), and along the curves given in figure 45, h_2/h_0 = constant - the values $\bar{c}_2$ and h_2/h_0 may be read off, and from (89b) we have h_0'/h_0 along these curves.

4. Points of fixed curves $h_0'/h_0 = k$ may also be directly computed. To each h_2/h_0 there corresponds with the assumed fixed ratio $h_0'/h_0 = k$, a value $\bar{c}_2$ from equation (89a). The intersection of the circle with this value of $\bar{c}_2$ as radius, and the origin as center with the corresponding h_2/h_0 curve gives a point of the required curve $h_0'/h_0 = k$.

By means of the methods given above the curves of constant energy were drawn in figure 46 and on chart 4.

Since in a gas the heat content after the shock at points of rest is still the same, the critical velocity which for an ideal gas is computed as

$$a^* = \sqrt{2g \frac{k-1}{k+1} i_0}$$

is a constant magnitude in the entire flow plane even when shocks occur.

In a water flow, however, it is to be observed that the analogous critical velocity for water is not constant, equation (42) being valid:

$$a_1^{*2} = \frac{2}{3} gh_0$$

This is constant only if the total head h_o is constant;
that is, in a flow without hydraulic jumps. If these oc-
cur, however, we have seen that the total head is constant
only between jumps, but for each discontinuity, "jumps"
to a new value h_o', so that at the same time there is a
jump in the critical velocity — the latter after the jump
assumes a new value a_2^*, which is smaller than a_1^*:

$$a_2^{*2} = \frac{2}{3} gh_o'$$

the ratio between the two being:

$$a_2^*/a_1^* = \sqrt{h_o'/h_o} \tag{90}$$

The change of the critical velocity (the limiting ve-
locity of streaming and shooting water) during hydraulic
jump, has the following important consequence:

Let the critical velocity before the jump be a_1^*;
the flow velocity c_1 (point P in fig. 47). After the
jump, let the velocity be c_2 (point Q). PQ is a shock
polar. As a result of the jump, the total head and hence
a_2^* have become smaler than h_o and a_1^*, respectively.
It may then happen that in case c_2 is also smaller than
a_1^*, c_2 nevertheless becomes larger than a_2^*. This
means that the water continues to shoot after the jump,
even if $c_2 < a_1^*$. There exists a curve $c_2/a_2^* = 1$ (fig.
47). According to whether the point Q is without or
within the area bounded by the curve and the u-axis, the
water, after the jump, is shooting or streaming. For a
gas this limiting curve, on account of $a_1^* = a_2^* = a^*$,
is a circle about O.

The curve $c_2/a_2^* = 1$ that holds for water, is found
in the following manner. Substituting in equation (89b)
the relation (90), we have:

$$h_o'/h_o = h_2/h_o + \frac{1}{3} h_o'/h_o \left(c_2/a_2^*\right)^2$$

Putting $c_2/a_2^* = 1$, there is obtained the equation:

$$h_o'/h_o = \left(\frac{3}{2}\right) h_2/h_o$$

From the family of curves $h_o'/h_o = $ constant, and $h_2/h_o =$

constant, that curve along which this relation is satis-
fied, is drawn. This is the required limiting curve.

Since hydraulic jumps occur in shooting water only,
two cases are possible: 1) Shooting water goes over after
the jump, into streaming water. 2) The flow is shooting
also after the jump.

All right hydraulic jumps are followed by streaming
water after the jump.

If the velocities are plotted in the characteristics
and shock diagrams to an absolute velocity scale, then to
each total head would correspond its own diagram. All
these would be similar to one another. If, however, we
plot the nondimensional velocities (referred, for example,
to a^*_1) only a single diagram is required. It is to be
observed, however, that in the shock diagram after the
jump (point Q), we deal with the velocity c_2 referred to
a^*_1. If, however, the further changes in velocity are de-
sired — whether of the characteristic diagram of a flow
without losses, or of a new jump — the velocity c_2 must
be referred to a^*_2, i.e., c_2/a^*_2. This is given in the
hodograph by the point Q' (fig. 47). It is obtained
from c_2/a^*_1 by multiplication by a^*_1/a^*_2, that is,
from (90):

$$c_2/a^*_2 = c_2/a^*_1 \sqrt{h_0/h_0'}$$

For this reason the curves of constant total head after
the jump (fig. 46 and chart 4) are denoted by $\sqrt{h_0'/h_0}$
instead of by h_0'/h_0 as parameter.

In order to avoid having to pass from Q to Q' af-
ter the jump $\overarc{PQ}$, the shock polar could also have been
defined as the geometric locus of all points Q' which
correspond to a fixed point P. There would thus be lost,
however, the property of the shock polars, that the nor-
mals to their chords are parallel to the shock wave front
in the flow.

20. Summary

We have seen that the flow of a compressible gas with
k = 2 for the case with shock is no longer analogous to
the flow of water on a horizontal bottom. From figure 46

it may be seen, however, that the energy loss $\Delta e = 1 - h_0'/h_0$ is extremely slight over a large region. For shocks (hydraulic jumps), for example, whose state after the shock is given by point Q lying in the hatched region, the relative loss is less than 1 percent. On account of this small shock loss the analogy of the two types of flow is still satisfied to a first approximation also for the case with shock.

In order to have a comparison there has been drawn on figure 48 a shock polar for water and the corresponding shock polar for a gas (k = 2). There is also given the corresponding characteristic - the same curve for gas with k = 2 and water - in order to show that for continually decreasing shocks, the two shock polars approach one another and tend to coincide with the characteristic.

ELEMENTARY SOLUTIONS OF FLOWS

For flows, bounded on two sides, in which hydraulic jumps occur, there are a number of problems which will be treated in this section.

There arises, for example, the question as to what occurs when a disturbance wave encounters a jump wave front. For the limiting case of a very small jump, this must naturally approach the case of two intercrossing disturbance lines. Other problems are the crossing of two hydraulic jumps of different families or the encounter of two jumps of the same family. Furthermore, it is possible for two flows of different directions that start from the same state of rest or from two independent states of rest, to meet. During this meeting it may happen that both are parallel flows in the same direction and form a vortex sheet at their surface of separation. Then there arises the further question as to what happens when a disturbance wave meets such a vortex sheet.

21. Level Drop about an Edge

Figure 26[*] shows the level drop about an edge as obtained by the characteristic method. In what follows, it will be directly computed for water, the computation being

---

[*]For figure 26, see Part I, T.M. No. 934.

the same as that carried out by Meyer for gases (reference 2).*

The origin of coordinates is taken through the edge S and the coordinate axes as shown in figure 49. In the three equations of continuity, irrotational motion, and energy, polar coordinates are substituted in order that the property of a flow about an edge - namely, that all magnitudes, as water depth h and velocity $c(c_r, c_t)$, on a ray through the edge are constant, may be simply expressed. The continuity equation (11) in polar coordinates is

$$\frac{\partial h c_r}{\partial r} + \frac{1}{r} h c_r + \frac{1}{r} \frac{\partial h \cdot c_t}{\partial \vartheta} = 0 \qquad (91)$$

The equation for the condition of no vorticity $\partial u/\partial y - \partial v/\partial x = 0$ becomes:

$$\frac{\partial c_t}{\partial r} + \frac{c_t}{r} - \frac{1}{r} \frac{\partial c_r}{\partial \vartheta} = 0 \qquad (92)$$

Expressing now the fact that all magnitudes are functions of ϑ alone, we obtain from (91) and (92), if we also add the energy equation (9), the three equations:

$$h c_r + \frac{d(h c_t)}{d\vartheta} = 0 \qquad (93)$$

$$c_t - \frac{d c_r}{d\vartheta} = 0 \qquad (94)$$

$$c_r^2 + c_t^2 + 2g h = 2g h_0 \qquad (95)$$

where c_r, c_t, and h are to be considered dependent variables. Eliminating c_r and ϑ, from the three equations, there is obtained:

---

*The flow will not be investigated in detail here, but mainly the change in the water depth on traversing a disturbance wave. Since for the disturbance waves the deflection angle of the velocity is the characteristic feature, there will also be determined the change of the water depth as a function of the velocity deflection.
**From (95) we have $c_r dc_r/d\delta + c_t dc_t/d\delta + g dh/d\delta = 0$. This multiplied by h and replacing $dc_r/d\delta$, according to (94), by c_t, gives: $h c_r c_t + h c_t dc_t/d\delta + gh dh/d\delta = 0$. Multiplying equation (93) by c_t and subtracting, there is finally obtained: $(gh - c_t^2) dh/d\delta = 0$.

$$c_t^2 = g\,h, \qquad c_t = -\sqrt{g\,h} \quad^* \tag{96}$$

The velocity component c_t, normal to the ray through the edge, is equal to the wave-propagation velocity (sound velocity in the gas). These rays are thus the Mach lines of one family.

Substituting (96) in (95) there is also obtained the radial component c_r of the velocity as a function of the water depth h:

$$c_r^2 = 2g\,h_0 - 3g\,h, \qquad c_r = +\sqrt{2g\,h_0 - 3g\,h} \quad^* \tag{97}$$

We now have also the angle ψ which the streamline forms with the straight ray through S:

$$\psi = (\tan^{-1})(c_t/c_r) = -(\tan^{-1})\sqrt{\frac{h/h_0}{2 - 3\,h/h_0}} \tag{98}$$

The flow is determined by (96), (97), and (98). We still require h as a function of ϑ. From (97)

$$\frac{dc_r}{d\vartheta} = \frac{dc_r}{dh}\frac{dh}{d\vartheta} = -\frac{1}{2}\frac{3g}{\sqrt{2gh_0 - 3g\,h}}\frac{dh}{d\vartheta}$$

Substituting (96) and the above equation in (94), there is found

$$d\vartheta = +\frac{3}{2}\frac{d(h/h_0)}{\sqrt{(2 - 3h/h_0)h/h_0}} = +\frac{\sqrt{3}}{2}\frac{d(3h/h_0 - 1)}{\sqrt{1 - (3h/h_0 - 1)^2}} \tag{99}$$

Integrating, there is obtained:

$$\vartheta = \frac{\sqrt{3}}{2}(\sin^{-1})(3\,h/h_0 - 1) + \text{constant} \tag{99a}$$

For the flow about an edge S starting from a parallel

---

*That the sign of c_t (96) must be negative may readily be seen. In figure 49 all magnitudes are so drawn that they have positive signs in the given coordinate system. The flow is from left to right, so that for it $c_t < 0$. For the same reason in (97) $c_r > 0$, as may also be found from the fact that the flow about the edge (decreasing ϑ) is equivalent to a jet expansion and that this in the case of shooting water must lead to a sinking in level as a consequence, so that the sign in equation (99) is correct.

flow with the Mach number $M = 1$, the constant is $\frac{\pi}{2}\left(1 - \frac{\sqrt{3}}{2}\right)$.

The velocity c forms with the direction of the x-axis an angle ω, where $\omega = \psi + \vartheta$, ω being the angle of deflection of the velocity from the direction of approach. Only because we had laid the x-axis in the direction of approach, is this deflection angle ω here equal to the angle φ of the velocity diagram. Figure 50 shows h/h_o as a function of ω (ψ equation (98) + ϑ equation (99a)) for the flow which starts with $M = 1$. The values are collected in table II (p. 53).

The change in the deflection angle is

$$d\omega = d\psi + d\vartheta$$

Taking $d\psi$ from equation (98):

$$d\psi = -\frac{d(h/h_o)}{2(1 - h/h_o)\,\sqrt{(h/h_o)\,(2 - 3\,h/h_o)}}$$

and $d\vartheta$ from equation (99), we have:

$$\frac{d\omega}{d(h/h_o)} = \frac{\sqrt{3}}{2}\,\frac{\sqrt{2/3 - h/h_o}}{\sqrt{h/h_o}\,(1 - h/h_o)} \tag{100}$$

This equation may also be obtained from equation (40a) if the expression $2gh_o - 2gh$ is substituted for c^2 since the velocity curve of a flow about an edge is a characteristic. The values computed from equation (100) are given in table III.

22. Refraction and Reflection of Waves at a Vortex Sheet

We shall assume that a flow (fig. 51) has a vortex sheet along AB. Above and below the sheet the flow is assumed parallel with the velocities c_{a_1} and c_{b_1}.* The water depths h_{a_1} and h_{b_1} are of equal magnitude. Furthermore, let the Mach numbers on each side of the vortex

---

*The first subscript (a, b) distinguishes the upper from the lower flow. The second subscript (1, 2, 3) denotes the corresponding field for the flow under consideration.

sheet be greater than 1. In the lower flow no disturbance
line is assumed. The line s is assumed to be a disturb-
ance line in the upper flow, and it meets the vortex sheet
at B.

We consider now the conditions that hold for all these
problems:

1. At each point of the flow and also at B, there
are two families of disturbance lines, so that from B
there can start out at most the two disturbance lines s'
and t'. The Mach line t cannot be a disturbance line be-
cause it lies upstream of the region of influence of the
the assumed disturbance s.

2. The velocities c_{a_3} and c_{b_3} must be parallel.

3. The water depth in the field a3 must be equal to
that in the field b3.

The above three conditions are sufficient to deter-
mine the angle of deflection produced by the refracted
wave s' and the reflected wave t' in the flow. For
small disturbances, we have:

$$\Delta h = (dh/d\omega) \, \Delta\omega; \quad \Delta h/h_0 = \frac{d(h/h_0)}{d\omega} \, \Delta\omega; \quad \left[\frac{d(h/h_0)}{d\omega} < 0 \right]$$

Hence

$$h_{a_2} = h_{a_1} + (dh/d\omega)_a \, \Delta\omega_{a_{12}} {}^{*} \tag{a}$$

$$h_{a_3} = h_{a_2} + (dh/d\omega)_a \, \Delta\omega_{a_{23}} \tag{b}$$

$$h_{b_3} = h_{b_1} + (dh/d\omega)_b \, \Delta\omega_{b_{13}} \tag{c}$$

In addition to these three equations, we have the condi-
tions:

$$h_{a_1} = h_{b_1} \tag{d}$$

$$h_{a_3} = h_{b_3} \tag{e}$$

$$\Delta\omega_{b_{13}} = \Delta\omega_{a_{13}}, \quad WO \tag{f}$$

where

$$\Delta\omega_{a_{13}} = \Delta\omega_{a_{12}} - \Delta\omega_{a_{23}} {}^{**} \tag{g}$$

---

*$\Delta\omega_{a_{12}}$ denotes the angle of deflection of the velocity
of flow a when it crosses the disturbance wave s from
region 1 into region 2. The $\Delta\omega$ are taken positive in the
direction in which the deflection lies if the wave under
consideration is a wave with level drop.
** (See p. 27)

From the above seven equations with the magnitudes:

$$h_{a_1}, \; h_{a_2}, \; h_{a_3}, \; h_{b_1}, \; h_{b_3}, \; \Delta\omega_{a_{12}}, \; \Delta\omega_{a_{23}}, \; \Delta\omega_{a_{13}}, \; \Delta\omega_{b_{13}},$$

$$(dh/d\omega)_a, \; (dh/d\omega)_b$$

where those underlined are to be considered as given, all the unknowns may be computed. In particular,

$$\Delta\omega_{a_{23}} = \Delta\omega_{a_{12}} - \Delta\omega_{a_{13}} \tag{101}$$

and

$$\Delta\omega_{b_{13}} = \Delta\omega_{a_{13}} = \Delta\omega_{a_{12}} \frac{2}{[1 + (dh/d\omega)_b/(dh/d\omega)_a]} \tag{102}$$

In the above formula $(dh/d\omega)_b/(dh/d\omega)_a$ will be made non-dimensional by introducing the total heads h_{o_a} and h_{o_b}.

$$\frac{\left(\dfrac{dh}{d\omega}\right)_b}{\left(\dfrac{dh}{d\omega}\right)_a} = \frac{\left(\dfrac{dh/h_o}{d\omega}\right)_b}{\left(\dfrac{dh/h_o}{d\omega}\right)_a} \frac{h_{o_b}}{h_{o_a}} = \frac{\left(\dfrac{dh/h_o}{d\omega}\right)_b \Big/ (h_1/h_o)_b}{\left(\dfrac{dh/h_o}{d\omega}\right)_a \Big/ (h_1/h_o)_a} = \frac{y_b}{y_a} \tag{103}$$

where y_b and y_a are written, for briefness, as the numerator and denominator, respectively. From equation (100)

$$y = \frac{2}{\sqrt{3}} \frac{1 - h/h_o}{\sqrt{h/h_o} \sqrt{\frac{2}{3} - h/h_o}}$$

Substituting the Mach number M in place of the water depth ratio h/h_o $(M^2 = c^2/a^2 = 2 h_o/h - 2)$, there is obtained:

$$y = \frac{M^2}{\sqrt{M^2 - 1}} \tag{104}$$

**(From p. 26)

Here we must subtract since if $\Delta\omega_{a_{12}}$ and $\Delta\omega_{a_{23}}$ have equal signs, s and t' are both rarefactions or both condensations. The angles of deflection of the velocity then act in opposite sense because s and t' are waves of different families.

Equation (102) may then be written, finally:

$$\frac{\Delta\omega_{a_{13}}}{\Delta\omega_{a_{12}}} = \frac{\Delta\omega_{b_{13}}}{\Delta\omega_{a_{12}}} = \frac{2}{1 + y_b/y_a} \qquad (105)$$

and equation (101) becomes:

$$\frac{\Delta\omega_{a_{23}}}{\Delta\omega_{a_{12}}} = 1 - \frac{\Delta\omega_{a_{13}}}{\Delta\omega_{a_{12}}} = \frac{y_b/y_a - 1}{y_b/y_a + 1} \qquad (106)$$

For clarification, two numerical examples will be computed:

According to equation		1. $M_a=2$, $M_b=3$	2. $M_a=3$, $M_b=2$
(104)	$y_a =$	2.31	3.18
	$y_b =$	3.18	2.31
	$y_b/y_a =$	1.33	.726
(105)	$\Delta\omega_{a_{13}}/\Delta\omega_{a_{12}} =$	+.84	+1.16
(106)	$\Delta\omega_{a_{23}}/\Delta\omega_{a_{12}} =$	+.16	-.16

These two examples are schematically represented in figure 52 for an approaching level drop wave as well as for a level rise wave. The numbers written beside the disturbance lines are the deflection angles referred to the deflection angle of the approaching disturbance.

We shall consider this behavior more in general. In figure 53, y is shown as a function of M. The expression $y = M^2/\sqrt{M^2 - 1}$ is to be investigated for $M > 0$.

1. y is real only for $M > 1$; y has no real zero.

2. $y \longrightarrow \infty$ a) for $M \longrightarrow 1$ as $y = 1/\sqrt{2(M - 1)}$

           b) for $M \longrightarrow \infty$ as $y = M$

3. $\dfrac{dy}{dM} = \dfrac{M(M^2 - 2)}{(M^2 - 1)^{3/2}}$ a) y has a minimum at $M = \sqrt{2}$ with $y = 2$

                 b) $\infty > M > \sqrt{2}$; y increases

                 c) $\sqrt{2} > M > 1$; y decreases

y is always positive $\infty > y > 2$. To each y there correspond two possible Mach numbers M. All possible ratios of any two values of y are positive: $0 < (y_b/y_a) < \infty$. Thus, according to equation (105)

$$0 < (\Delta\omega_{a_{13}}/\Delta\omega_{a_{12}}) < 2$$

This means that the wave passing through and refracted by the vortex sheet, is of the same type as the incident wave and has up to twice as large a deflection angle as the incident wave. Furthermore, the reflected disturbance line, on account of $-1 < (\Delta\omega_{a_{23}}/\Delta\omega_{a_{12}}) < +1$, has at most the same deflection as the incident disturbance, but may be of the same or opposite sign. The following table summarizes the various possible cases:

$$y_a = M_a^2/\sqrt{M_a^2 - 1}, \quad y_b = M_b^2/\sqrt{M_b^2 - 1},$$

$$p = 2/(1 + y_b/2) \quad \text{and} \quad q = 1 - p, \quad 0 < p, q < 1)$$

$M_a > 1, M_b > 1$	$\Delta\omega_{13}/\Delta\omega_{a_{12}}$	$\Delta\omega_{a_{23}}/\Delta\omega_{a_{12}}$
I. $M_b > \sqrt{2}$ 1. $M_a < \sqrt{2}$ a) $y_a > y_b$	2 to 1	-1 to 0
b) $y_a < y_b$	1 " p	0 " q
2. $M_a > \sqrt{2}$ c) $y_a < y_b$	p " 1	q " 0
d) $y_a > y_b$	1 " 2	0 " -1
II. $M_b < \sqrt{2}$ 1. $M_a < \sqrt{2}$ e) $y_a > y_b$	2 " 1	-1 " 0
f) $y_a < y_b$	1 " p	0 " q
2. $M_a > \sqrt{2}$ g) $y_a < y_b$	p " 1	q " 0
h) $y_a > y_b$	1 " 2	0 " -1

In figure 54 are shown several clarifying sketches. The first series holds for $M_b > \sqrt{2}$, the second for $M_b < \sqrt{2}$. The numbers beside the disturbance lines are the values $\Delta\omega/\Delta\omega_{a_{12}}$. Since the equation

$$M_a^2 / \sqrt{M_a^2 - 1} = M_b^2 / \sqrt{M_b^2 - 1}$$

has the two positive solutions

and
$$M_a = M_b$$

$$M_a = M_b / \sqrt{M_b^2 - 1}$$

there are two cases for which a disturbance wave passes through the vortex sheet without any reflection. The first case is self-evident. The two flows a and b are equal to each other. In the second case, however, a vortex sheet is present. Nevertheless the disturbance wave is not reflected but passes through - though refracted - and has before and after, the same deflection angle for the velocity.

Since the hydraulic jump loss is still small, even for rather large jumps, the ratio of the Mach numbers on the encounter of two flows that arise from the same state of rest, and of which one has experienced a jump while the other is without loss, is in the neighborhood of one. y_a is then approximately equal to y_b and it follows from equations (105) and (106) that the main portion of the incident waves goes through the vortex sheet and only a much smaller part is reflected.*

23. Flows with Hydraulic Jump

a) <u>Critical angle</u>.- To each Mach number M, or to each nondimensional velocity $\bar{c}$, before a hydraulic jump (shock), there corresponds a shock polar to which a tangent may be drawn from the origin. The angle between this tangent and the u-axis is the maximum angle by which the flow with the corresponding Mach number may be deflected.

----

*A numerical example that illustrates this is the following: 1. $M_a = 1.75$; 2. $h_0'/h_0 = 0.95$ for the flow which experiences a jump. Then with $h_{b_1} = h_{a_1}$ and h_{b_1}/h_0', we have $M_b = 1.68$. With these two Mach numbers, there is obtained from equations (104), (105), and (106), depending on whether a disturbance wave meets the vortex sheet from below or above:

$$(\Delta\omega_{13}/\Delta\omega_{12}) = 0.99, \text{ and } 1.01, \text{ respectively}$$

and
$$(\Delta\omega_{23}/\Delta\omega_{12}) = 0.01, \quad " \quad -0.01, \qquad "$$

For if the angle of deflection were larger, the jump could no longer go past the edge but would travel upstream of the edge. If the side boundaries are infinitely long, it travels upstream to infinity and only streaming water remains at the edge (subsonic flow). If the boundary of the deflected jet is finite (see fig. 85), the jump also travels upstream for the above critical angle but always remains at a finite distance from the obstacle.

Besides the critical angle, which indicates whether a jump is at all possible, there is another somewhat smaller limiting angle, also depending on the Mach number of the flow - namely, the deflection angle, for which the Mach number M after the jump, is exactly equal to 1. (See also fig. 47.) In figure 56, the critical angle is shown as a function of the nondimensional velocity $\overline{c}_1$ before the jump.

b) <u>Hydraulic jump impinging on a fixed wall</u>.- If a jump, for example, as a wave of the lower family, impinges on a fixed wall, only waves of the upper family can start out from there. The reflected waves must make the velocity after traversing the incident, and reflected waves have the same direction as before the incident wave. From this it follows that the reflected wave must also be a jump with the same deflection angle as the incident wave. Figure 55 shows an example. Let the incident jump be characterized by the jump AB on the shock polar through A. BB' is the change in velocity due to the jump loss; see also figure 47. We then have the jump $B'C$, and finally, the adjustment CC'

In flows with hydraulic jump, in addition to the two field coordinates, we need the depth referred to a fixed depth (for example, that of the approach flow) as a third coordinate, in order that the depth lines of the water surface may be drawn.

As for the simple slant jump, there is also for each Mach number a critical angle which indicates the upper limit of the deflection of the jump against the wall in order that reflection may be possible.

In figure 55 is drawn the limiting curve, outside of which the impinging jump must lie in order that reflection may be possible. There is also shown, with the aid of an example, how this limiting curve is found. It is determined by the condition that the reflected jump gives rise to its

greatest possible deflection. The critical reflection an-
gle of the reflected jump is approximately half as large
as for the ordinary jump (fig. 56).

c) _Hydraulic jump impinging on a free jet boundary._-
At the free jet boundary the pressure must be constant.
This condition is satisfied if, at the position where the
jump strikes, a family of waves with level drop starts
out. If the jump were free from losses, the deflection of
the velocity at the free jet boundary would be twice as
large as the deflection by the incident jump, and the mag-
nitude of the velocity would not change. Actually the de-
flection is somewhat smaller, depending on the losses and
the velocity decreases.

d) _Encounter of two hydraulic jumps of different fam-_
ilies (crossing).- Whereas, for the impact of a jump
against a fixed wall, only a single condition on the direc-
tion must be satisfied, and for an impact against a free
jet boundary, only a condition on the pressure, in the case
of the intercrossing of two jumps, conditions on both the
pressure and direction must be simultaneously satisfied.
Only if the angles of deflection of the two intercrossing
jumps are equally large, does the problem lead to a con-
dition on the direction only and hence to case (b).

The solution of the general case is obtained by trial.
The direction of the velocity, after the two jumps, is ob-
tained to a very good approximation if the jumps are con-
sidered as though there were no impact losses. For the
determination of the water depths and the velocity on the
hodograph, the four different impact losses may subsequent-
ly be read off and corrected for. For drawing accuracy
this is entirely satisfactory. In what follows, we shall
consider the process theoretically in somewhat greater de-
tail (fig. 57).

In the velocity diagram, let the impact coming from
above be given by AB, the corresponding adjustment by
BB', and the impact striking from below, by ACC'. After
the crossing, there is a jump, C'EE' on one side, and
B'DD' on the other. The points D' and E' must, on
the one hand, lie on the same ray through O, and on the
other hand, the water depth for D' (losses of A after
B, and of B' after D); and the water depth for E'
(losses of A after C, and of C' after E), must be
equal to each other. Since, however, the product of the
values h_o'/h_o for the jumps AB and B'D with very

great accuracy is equal to the product of the values h_o'/h_o
for the shocks AC and C'E, the points D' and E' co-
incide; and furthermore, the vortex sheet starting from
the crossing position, is very weak.

e) <u>Encounter of two hydraulic jumps of the same family
(overtaking)</u>.- The jump AB with the adjustment BB' and
the succeeding jump B'CC' are given by the deflection an-
gle of the wall (fig. 58). The two impacts are waves of
the same family (in the example, the lower one). They meet
at the point P of the flow. All possible waves which
pass through this point are drawn. At this point we have
a meeting of: 1) the two given impacts; 2) the Mach lines
a, b, c, and d - the latter causing no disturbances. From
P there start out: 1) the resultant impact PQ; and 2)
the disturbance line PR. The streamline passing through
P is obtained as a vortex sheet in its upstream lying
portion. The impact PQ and the wave PR are determined
by the condition that, above and below this vortex sheet
the water depths and velocity directions agree; i.e., the
points E' and D of the velocity diagram must lie on the
same ray through O, and $h_{E'}$ must be equal to h_D. The
impact losses for the two jumps AB and B'C following
each other are, together, smaller than the single impact
loss of the jump AE. (If, instead of two discontinuous
deflections, there were many very small ones, the lower
flow would finally pass over into a flow without dissipa-
tion, while there would always start out a finite jump
with dissipation, from the meeting point of all the dis-
turbance lines.) The product of the values h_o'/h_o for
the jumps AB and B'C, is thus nearer one than h_o'/h_o
for the jump AE. For this reason, E' must lie nearer
the origin O of the velocity diagram than D.

In the example computed, the result was obtained that
the disturbance PR (line of the upper family) is a level
drop wave to which, in the velocity diagram, corresponds
the characteristic C'D. The deflection caused by it is
very small compared to the two changes in direction due to
the jumps. In most cases the overtaking of two jumps is
also computed with good approximation by superposing the
deflection angles upon each other.*

---

*In the example the first deflection of the wall is 19.4^o,
the second, 6.8^o. The velocity deflection by the result-
ant jump is 27.3^o. If the deflection angles of the two
jumps were simply added and the sum taken as the deflec-
tion of the resultant jump, the error would have been 1°
in 25°.

f) _The three possible cases of the encounter of dis-_
turbance waves with hydraulic jumps.- Figure 59 shows the
three possible cases: 1), 2), and 3). In the first case
the disturbance line crosses the jump. This is a limit-
ing case of the intercrossing of two jumps (section d).
Practically, there occurs no vortex sheet, and after the
crossing both the jump and the disturbance wave deflect
the velocity with extraordinary accuracy by the same angle
as before the encounter.

The second and third cases are both limiting cases of
the overtaking of two hydraulic jumps. Here, too, the de-
flections may be approximately superposed, which means that
the reflected wave PR is neglected compared to the inci-
dent wave.

An idea as to the strength of the vortex sheet and the
order of magnitude of the reflection PR may be obtained
by a simple consideration. The disturbance line meeting
the jump is imagined as a zero-loss rarefaction of the
same deflection angle of the velocity as the jump. This
rarefaction is assumed to be concentrated on a single line
(fig. 60) which, of course, is not actually the case. If
the shock polars were characteristics and the jumps were
without losses, the jump and the disturbance would then
balance each other at point P, from which point there
would not start out then any jump PQ, disturbance line
PR, or vortex sheet. For the actual jump these lines do
not vanish, however, and from them an estimate may be made
of the order of magnitude of the reflection that occurs if
only a small disturbance strikes against the slant hydrau-
lic jump.

Figure 60 shows these relations by an example (case
3). On crossing the jump from region A to region B in
the flow, the state in the velocity diagram jumps from A
to B on the shock polar AB with the corresponding im-
pact loss. To B is added the adjustment BB'. From re-
gion B to C, a zero-loss rarefaction is crossed which
by assumption is concentrated on a single line, and whose
deflection brings the velocity into the direction before
the jump. Crossing this rarefaction means for the condi-
tions in the velocity diagram a traveling on the character-
istic B'C. The waves PQ (lower family) with the ini-
tial point A, and PR (upper family) with the initial
point C, must bring about the condition that in the re-
gions E and D of the flow which are separated by the
vortex sheet starting from P the pressure and direction

of flow are equal. These conditions determine D and E
in the velocity diagram lying on the characteristics CD,
and AE, respectively.

The reflected wave PR (level rise), and the wave
PQ (drop), which in the case of equal and opposite de-
flection angles at the corners S and T give the devi-
ation from simple superposition of the deflection angles,
are both very small compared to the wave TP overtaking
the jump.*

g) Summary.- All flow elements with hydraulic jump
have the common property that a vortex sheet arises which
may generally be neglected. To satisfy the conditions of
equality of pressure and direction on the two sides of
the vortex sheet, two waves are developed whose deflec-
tions are determined from these conditions. Especially
striking is the case where jumps overtake other jumps or
disturbance lines since in this process all given waves
are of the same family; nevertheless, small waves arise of
the other family.

h) Application.- Let shooting water (M = 2) flow in
a channel of 24° deflection.** Let the deflection be facil-
itated through a vane at the center of the channel, so that
the banking of water on the concave side of the wall may be
reduced (fig. 61). The contour of the vane is on the upper
side made up of a circular arc with short straight pieces
at the ends and a straight line at the lower side making
an angle of 12° to the direction of approach. The lower
wall of the channel is assumed to be a circular arc. The
upper (left) boundary of the channel is determined so
that the flow at the upper side of the vane is without
losses and at the end of the vane there is again produced
a parallel flow with M = 2. This side of the flow is
thus a clear channel which deflects a parallel flow in the
simplest manner.

At the end of the vane at both sides, arises a hy-
draulic jump since the vane angle there is not zero.

---

*In the example of figure 60, the jump angle is about 25°
for $h_0'/h_0 = 0.90$. The impinging wave has the same change
in direction of the velocity (25°). The deflections of
the reflected jump and of the deviation, however, amount
to only 1°. Only 4 percent of the waves overtaking the
jump are reflected.
**Th. v. Karman (reference 4) in 1938, considered the de-
flection in an open run analytically.

These two jumps are determined from the pressure and direc-
tion conditions for the upper and lower sides of the stream-
line starting from the trailing edge.

X-SURFACES

As previously remarked, the position-determining poten-
tial itself is not required if the velocity diagram and the
flow are drawn simultaneously. We wish, however, to see
what the appearance of the X-surfaces (formulas 24-31) of
several flows is like.

24. Parallel Flow

In the entire field of flow the velocity components
u and v have the fixed values u_0, v_0. On account of

$$d\chi = \chi_u \, du + \chi_v \, dv = x \, du + y \, dv$$

χ thus has a fixed value χ_0. The points of the χ-surface
all coincide at the single point u_0, v_0, χ_0. The slope
of the χ-surface, however, is not constant, being given
according to equations (24a) by the coordinates x and y
of the flow: $\chi_u = x$; $\chi_v = y$. For an infinitely wide par-
allel flow, it thus takes on all values.

For the χ-surface of a parallel flow, we find a bun-
dle of infinitely many plane elements through a point.
The reason why this χ-surface degenerates so strongly is
to be found in the fact that the inverse transformation
from the velocity field (χ, u, v) to the flow space
(Φ, x, y) for a parallel flow is infinitely many-valued.
All flows whose transformations to the velocity space are
not reversible (parallel flow and flow bounded on one
side), have degenerated χ-surfaces. Although in these
cases Φ, x, y do not inversely give uniquely χ, u, v
there corresponds to each element Φ, x, y, Φ_x, Φ_y of the
Φ-surface a quite definite element χ, u, v, χ_u, χ_v of the
χ-surface and conversely.

25. Laval Nozzle for M = 2

The χ-surface for the experimentally investigated Laval

nozzle (fig. 77) is shown in figure 62.. Its only discon-
tinuities lie at the boundary since to each point u,v in
the interior there corresponds uniquely a point of the
flow. In particular, A and B are points of the type
described in section 24.

26. Orifice

We wish to consider the flow out of an orifice with
small back pressure (fig. 63). Let the parallel flow of
approach in the minimum cross section have the velocity
$c = a^*$, so that $\bar{c} = 1$. To this there corresponds in the
velocity diagram, the point A'. The first Mach line
which starts from P strikes the edge Q. The first dis-
turbance line, however, that starts from P or Q, strikes
the symmetry axis in R (not in A), depending on the mag-
nitude of the increments that are chosen for the disturb-
ances. The level sinking about the edge P has no effect
at the edge Q, and conversely. We first have about each
edge in its immediate neighborhood a normal level drop
bounded on one side (sec. 21); the disturbance waves start-
ing out from P, for example, are given by the normals to
the characteristic A'B' (depending on the chosen incre-
ment of the deflection angle). Analogously, the states
at Q are given on the characteristic A'B". The level
sinking proceeds up to points such as B' and B", whose
speeds OB' = OB", according to the energy equation, cor-
respond to the given lower water depth. (For a gas the
expansion proceeds until the prescribed back pressure is
attained.) The usual flow about an edge (flow bounded at
one edge) holds until it impinges on the first disturbance
line RS or RT (fig. 63). From there on the crossing
family of disturbance lines is constructed as for the Laval
nozzle. Along the AX axis the velocity is horizontal for
reasons of symmetry. In the velocity diagram it changes
from A' to X'. It is further to be remarked that at X
the water depth is as great as it would be for a one-side
bounded flow about an edge if the flow had twice as large
a deflection as that about P or Q. Although the dis-
turbance lines (straight rays) of the one-side bounded
flows about P and Q are not superposed simply as such,
the angles of the velocity deflections are, however, super-
posed. The processes at each side of the axis are such as
though the axis were a fixed wall, as must be the case
since each streamline may be considered as a fixed wall.

The origin of the coordinate system x,y is placed
in the orifice cross section and in the channel center

(point A of fig. 63). All points of the orifice cross section PAQ have, in the velocity diagram, the single image point A'. Since along the entire distance PAQ $x = 0$, the χ-surface at A' in the direction of the $\bar{u}$-axis, is horizontal. In the direction of the $\bar{v}$-axis, however, it has at A' all slopes between $- y_0 < \chi_v < + y_0$. Since there is no constant value for χ, we shall set χ at A' equal to zero.

To the point Q of the flow, there correspond all points of the characteristic A'B" of the velocity diagram. The χ-surface is thus of such character that for all points of A'B", it has the slopes $\chi_u = 0$ and $\chi_v = + y_0$. The edge of the χ-surface, whose projection is the characteristic A'B", thus lies in a plane. The latter has, in the $\bar{v}$ direction, the slope y_0, and since we have set χ in A' equal to zero, it passes through the $\bar{u}$-axis. With its points vertically above A'B", it gives not only points of the χ-surface but also the tangent plane to the surface at these points. Similarly, the plane through the $\bar{u}$-axis with the slope $\chi_v = - y_0$ gives symmetrically points over A'B', together with the tangent plane of the χ-surface. Furthermore, this surface has, above the $\bar{u}$-axis, a horizontal tangent in the $\bar{v}$-direction since the velocities along the $\bar{u}$-axis ($\bar{v} = 0$) in the flow occur on the channel axis and where $y = 0$.

The χ-surface appears as a valley between the two planes described above, ending at A', and which in all sections $\bar{u} = $ constant ranges through all slopes $- y_0 < \chi_v < + y_0$.

Particularly noteworthy is the behavior of the χ-surface with regard to the point A'. The values of χ itself are continuous. The slope in the $\bar{v}$ direction, however, becomes discontinuous in A' since, although the surface ends continuously in a point, the slope still has all values between $\chi_v = - y_0$ and $\chi_v = + y_0$ (fig. 64).

27. χ-Surface of the Flow about an Edge

Since the flow about an edge is a flow bounded on one side, and since it is discontinuous at the edge, its χ-surface degenerates.

Since all the velocity vectors have their ends on a single characteristic, the latter is the projection of the

χ-surface. If, furthermore, we place the origin of the co-ordinate system x,y in the edge S (fig. 49), then for all points of the hodograph corresponding to S ($x = 0$, $y = 0$) - i.e., for the entire characteristic, on account of $d\chi = \chi_u du + \chi_v dv = x\,du + y\,dv$, $d\chi = 0$; that is, $\chi = $ constant $= \chi_0$. The portion of the χ-surface correspond-ing to the point S is thus a curve lying vertically above the characteristic at a constant height or, more accurate-ly, an infinitely narrow horizontal strip.

Furthermore, along a fixed ray through S the veloc-ity components u and v are constant and therefore (again on account of $d\chi = x\,du + y\,dv$), $\chi = $ constant $= k$ for each ray through the edge S. The constant k for all rays has at the edge, however, the constant value $k = \chi_0$. Thus for the entire flow about an edge, $\chi = \chi_0$. Since there is no constant value for the position-determin-ing potential, we may set $\chi_0 = 0$. The χ-surface shrinks into a characteristic.

To a fixed ray through the edge there corresponds, in the velocity diagram, a single point of the characteris-tic. Since along this ray y/x and hence χ_v/χ_u is con-stant, but χ_u and χ_v themselves are variable, the χ-surface at this point consists of a bundle of surface ele-ments.

The χ-surface of the total flow about an edge con-sists of a bundle of infinitely narrow surface strips which lie along a fixed characteristic in the u,v plane (fig. 65).

EXPERIMENTAL INVESTIGATIONS

TEST SET-UP

28. Measuring Channel

The tests were conducted at a flow tank of the Aero-dynamic Institute of the Swiss Technical High School at Zurich. The water used in the test was circulated by a pump which delivered up to about 25 dm^3/s. Figure 66 shows the test set-up. At 1 the water from the pump enters the tank. Through a screen 2, it is calmed and reaches the straightening section 2, 3 on the lower side of the inter-mediate bottom BB. At 3 and 4 are deflecting vanes. The

water, after two deflections, reaches the honeycomb 5.
There the velocity is small compared to the velocities in
the test portion, the water being led from the approach run
6, where it is greatly accelerated, to the Laval nozzle in-
vestigated 7. The condition of a quiet flow of approach
is thus attained and the measurement of the total energy in
the minimum cross section actually shows that, except for
points in the immediate neighborhood of the bottom and side
walls, the total energy has a constant value over the cross
section to within 1 percent.

Figure 67 shows the investigated Laval nozzle 7 as
seen from above, and figure 68, as seen from the nozzle
end. There may also be seen the two side walls of the flow
tank. In the background may be seen the honeycomb.

29. Measurement of the Depth

The shape of the surface (surface in space) of the wa-
ter flowing through the Laval nozzle was obtained by gaging
with a fine point (fig. 68). A horizontal cross beam on two
accurately horizontal longitudinal beams and normal to them,
is movable parallel to itself in the longitudinal direction
of the channel. On the cross beam is mounted a block, to
which the point movable in the vertical direction is fixed.

Gaging with the pin point gives measuring values which
are accurate to at least 1/10 millimeter and may be well
observed since on the finest contact with the surface of
the moving water, capillary waves are set up.

30. Measurement of the Total Energy and
of the Boundary Layer

In the theory of the characteristics method it was
assumed that the flow was frictionless. In the actual
flow, both at the bottom and at the side walls, boundary
layers are formed as a result of the friction. In order
to avoid the resulting deviation from the theory, the side
walls used in computing the flow were displaced inwardly
with respect to the actual (material) walls of the nozzle
by the boundary-layer thickness. Only a parallel displace-
ment is necessary since the mean thickness of the boundary
layer over the depth from the minimum cross section to the
nozzle outlet only slightly increases. (See fig. 73b.)
Furthermore, the bottom was not laid horizontal but slight-
ly inclined to correspond to the increase in the bottom
boundary layer.

Figure 69 shows the set-up for the determination of the total energy. The cross beam of the coordinate apparatus runs across the picture, and to the left may be seen a portion of a longitudinal beam. On the cross beam from left to right are:

1. The micrometer screw to which in the depth measurements a point has been clamped and provided with a support, to which is fixed a glass pitot tube. The distance of the tube from the bottom may thus be adjusted. This fine adjustment is used for the measurement of the bottom boundary-layer thickness.
2. To the same block, displaceable along the cross beam, is fixed a second micrometer screw which displaces a needle vertically, for measuring the height of the water in the pitot tube.

3. Finally, on the right is seen the mounting and adjustment of the block which is used for measuring the boundary layer at the vertical side walls of the nozzle.

BOUNDARY LAYER

31. Differential Equation of the Laminar Boundary Layer with Affine Velocity Profiles in a Constant-Width Channel

Let h denote the depth of the water (fig. 70), c the undisturbed velocity at the position x, δ the boundary-layer thickness, and p the pressure in the boundary layer. dh, dc, $d\delta$, and dp are the changes in these magnitudes in passing from the position x to the position $x + dx$. The width b of the channel is assumed constant and equal to unit length. Furthermore, let c'/c be set equal to ξ and $z/\delta = \eta$. Then for a boundary layer with affine velocity profiles, $\xi = f(\eta)$ is a curve independent of c and δ, and the magnitudes α, β, γ defined by the following expressions:

$$\alpha = \int_0^{\eta > 1} (1 - \xi)\, d\eta = \int_0^1 (1 - \xi)\, d\eta$$

$$\beta = \int_0^{\eta > 1} (1 - \xi^2)\, d\eta = \int_0^1 (1 - \xi^2)\, d\eta$$

$$\gamma = (d\eta / d\xi)_{\eta = 0}$$

are constants.independent of x. From these are computed:

The volume boundary-layer thickness $\delta_v = \alpha \delta$

The "momentum boundary-layer thickness" $\delta_i = \beta \delta$ (fig. 71)

The tangent intercept $\delta_T = \gamma \delta$ (fig. 71).

An important result is obtained from the continuity equation in connection with the energy equation. At the position x in the boundary layer and in the undisturbed flow, the same amount of fluid flows through as at x + dx, so that

$$c (h - \delta_v) = \text{constant}$$

or in differential form:

$$c (h - \delta_v) = (c + dc) (h + dh - \delta_v - d\delta_v) \qquad (107)$$

By the energy equation (9)

$$c \, dc = - g \, dh \qquad (108)$$

there is obtained, eliminating dc

$$dh = \frac{d\delta_v}{1 - \frac{g(h - \delta_v)}{c^2}} \qquad (109)$$

As long as the volume boundary-layer thickness is small by comparison with the water depth h, we may set $h - \delta_v \approx h$. Using also the relations $g h = a^2$ and $c/a = M$, equation (109) becomes, on dividing both sides by dx,

$$\frac{dh}{dx} = \frac{M^2}{M^2 - 1} \frac{d\delta_v}{dx} \qquad (110)$$

or, with (108),

$$\frac{dc}{dx} = - \frac{g}{c} \frac{M^2}{M^2 - 1} \frac{d\delta_v}{dx} \qquad (111)$$

The slope (dh/dx) of the water surface certainly never actually becomes infinite. Since, however, the denominator at the right for M = 1 assumes the value zero, in

order that the left sides of equations (110) and (111) may remain finite, the boundary-layer slope $d\delta_v/dx$ for those values of M must have the value zero. The points for $M = 1$ are the critical points; i.e., those where the flow velocity c is equal to the wave propagation velocity $\sqrt{gh}$. The boundary layer varies in such a manner that its thickness δ_v in the neighborhood of the critical positions neither increases nor decreases in the direction of the flow.

While normally a flow (for example, as a potential flow) is determined by the boundary walls (boundary conditions), and this flow then determines the course of the boundary layer, the relations at the critical points, on account of the great sensitivity of the flow to cross-sectional changes, are just the reverse. In this case the boundary layer acts as a determining factor on the flow.

We shall now apply the momentum equation to a portion of the boundary layer. Let the elementary region to which the equation is applied be bounded by the contour shown in figure 70 by the thick line: bottom, vertical at $x + dx$; boundary layer outer limit, vertical at x. The volume per second flowing at x into the region is:

$$V_x = c \, (\delta - \delta_v) = c \, (\delta - \alpha\delta) = (1 - \alpha) \, c \, \delta$$

The volume per second flowing at $x + dx$ out of the region is

$$V_{x+dx} = (1 - \alpha) \, (c \, \delta + d \, [c \, \delta])$$

Thus the volume per second flowing through the upper side of the region is

$$dV = V_{x+dx} - V_x = (1 - \alpha) \, (c \, d\delta + \delta \, dc) \qquad (a)$$

This quantity transfers through the upper side a momentum in the x-direction:

$$di_1 = c \, \rho \, dV = (1 - \alpha) \, \rho \, c \, (c \, d\delta + \delta \, dc) \qquad (b)$$

The momentum flow through the vertical side at x is:

$$i_x = \int_0^\delta c' \, \rho c' \, dz = \rho c^2 (\delta - \delta_1) = \rho c^2 (\delta - \beta\delta) = 1 - \beta) \, \rho c^2 \delta$$

Similarly there is obtained the outflowing momentum through
the vertical side at x + dx:

$$i_{x+dx} = (1 - \beta) \rho (c + dc)^2 (\delta + d\delta)$$

Hence the total momentum flowing into the region through
the vertical sides, is

$$di_2 = i_x - i_{x+dx} = - (1 - \beta) \rho c (c\ d\delta + 2\delta\ dc) \qquad (c)$$

Through the bottom surface no momentum enters the region.

   The external forces acting on the elementary region
under consideration in the x-direction are: 1) at the ver-
tical side at x: $\rho g (h - \delta/2) \delta$; 2) at the vertical side
at x + dx: $- \rho g \left(h + dh - \dfrac{\delta + d\delta}{2}\right) (d + d\delta)$; 3) at the
upper side: $\rho g \left(h + \dfrac{dh}{2} - \delta - \dfrac{d\delta}{2}\right) d\delta$; and 4) at the bot-
tom: $\tau\ dx$ where τ is the shear stress of the fluid at
the bottom at the position x. All these forces have, as
the resultant force in the x-direction, the sum:

$$dK = - \rho g\ \delta\ dh - \tau\ dx \qquad (d)$$

We may now write the momentum equation, which states that
the rate of change of momentum in the region corresponds
to a force that balances the external forces:

$$(1-\alpha)\ \rho c(cd\delta+\delta dc) - (1-\beta)\ \rho c(cd\delta+2\delta dc) = + \rho g\ \delta\ dh + \tau\ dx \qquad (e)$$

For the shear stress, we have:

$$\tau = \eta \left(\frac{dc'}{dz}\right)_{z=0} = \eta c / \delta_T = v \rho c / \delta_T = \frac{v \rho c}{\gamma\ \delta} \qquad (f)$$

(η is the dynamic viscosity, $\eta / \rho = v$, the kinematic vis-
cosity.) Between the depth of the water and the velocity,
holds the energy equation (108):

$$c\ dc = - g\ dh \qquad (g)$$

Substituting (f) and (g) in (e), there is obtained the dif-
ferential equation of the boundary layer:

$$\gamma\ (2\beta - \alpha)\ \delta^2 \frac{dc}{dx} + \gamma\ (\beta - \alpha)\ c\ \delta\ \frac{d\delta}{dx} = v \qquad (112)$$

This equation states that the rate of increase of the boundary-layer thickness decreases as the flow is more accelerated. For very large accelerations the thickness even decreases.

32. The Behavior of the Boundary Layer in the Throat Section of the Laval Nozzle

If we consider the Laval nozzle at the minimum cross section (throat), we have approximately the relations in a channel of constant width. At a short distance ahead of the section $M < 1$; that is, $M^2 - 1 < 0$, so that from equation (110), if the boundary-layer thickness increases $(d\delta_v/dx > 0)$, the water surface drops $(dh/dx < 0)$, and conversely. If the boundary layer would continue to increase toward the critical positions instead of remaining constant as we have seen from (110), the water level there would drop more sharply. The more it drops, however - that is, the greater the acceleration, the smaller the increase in the boundary layer. A balanced condition is thus obtained, when the level at the minimum section drops so rapidly and the acceleration becomes so large that the boundary-layer thickness no longer increases. There thus remains an inclination of the water surface even if the side walls at the minimum cross section have a small curvature and all effects of the latter vanish.

If, in equation (112), for dc we substitute dh from equation (108), we have:

$$- \gamma(2\beta - \alpha) \, \delta^2 g \, \frac{dh}{dx} + \gamma(\beta - \alpha) \, c^2 \delta \, \frac{d\delta}{dx} = v \, c \qquad (113)$$

From the above we obtain with $d\delta/dx = 0$ for the minimum cross section a relation between the slope of the surface and the boundary-layer thickness:

$$\frac{dh}{dx} = - \frac{v \, c}{\gamma(2\beta - \alpha) \, g \delta^2}$$

where $c = a = \sqrt{2g \, h_0/3}$. We then have:

$$\frac{dh}{dx} = - \frac{2\sqrt{2}}{\sqrt{3}} \frac{v \, \sqrt{h_0}}{\sqrt{g} \, (2\alpha\delta)^2} \frac{1}{\frac{\gamma}{2\alpha} \left(2 \, \frac{\beta}{\alpha} - 1\right)} \qquad (114)$$

A similar relation holds for a gas, the surface slope being replaced by a pressure drop.

33. Tests on the Boundary Layer in the Throat Section

The velocity profile of the flow at the channel center on the bottom was obtained for various total heads (variable discharge quantities). The results are shown in figure 71; δ_V denoting the volume boundary-layer thickness, δ_T the intercept of the tangent of the velocity profile, and δ_i the momentum boundary-layer thickness.

The averaged test values from figure 71 substituted in equation (114) give dh/dx as a function of h_o. This is the continuous curve of figure 72.

The slope of the water surface at the center of the minimum cross section was also directly measured, these test points also being plotted in figure 72.

34. Boundary-Layer Variation at the Side Walls

Figure 73a shows the contour lines of the total measured boundary-layer thickness at the side walls. On figure 73b is plotted the variation of the values averaged over the water depth along the walls. The boundary-layer thickness is practically constant and only increases somewhat at the end of the nozzle. The side walls of the nozzle used in computing by the characteristics method are shifted inward with respect to the real walls by the amount of this thickness.

35. Bottom Boundary Layer

Figure 74 shows the contour lines of the measured boundary-layer surface at the bottom. If this "hill" is replaced by a mean plane the latter has a slope in the longitudinal direction of the nozzle of 0.8 mm/m. The bottom of the nozzle was inclined by this amount, thus approaching more closely the theory which assumes a horizontal bottom for frictionless flow.

From figure 74 it may be seen, furthermore, that in the region of the minimum cross section the slope of the surface is extremely small in the direction of the flow, as must be the case according to previous consideration.

TEST RESULTS OF THE DEPTH MEASUREMENTS

36. Hydraulic Jump (Shock)

In a series of preliminary tests, measurements were also made on the hydraulic jump. The velocity of approach at a corner had the Mach number $M = 2$ (exit from the nozzle). For various deflection angles β (see fig. 37), the angle γ of the shock-wave front and the mean water depth h_2 at some distance after the shock, were measured. The test results are shown in figure 75.

37. The Water Depths in the Minimum Cross Section

Theoretically, the water-depth ratio at the minimum cross section h^*/h_0 should assume the value 2/3. Figure 76a shows the direct measurement of the water surface for various total heads along the channel center in the region of the minimum cross section. From this measurement were also taken the values dh/dx which were used in section 33.

On figure 76b are plotted the measured water depths h^* as a function of h_0. For all total heads that are somewhat smaller than 10 cm, i.e., for the ratio

$$\left(\frac{\text{total head } h_0}{\text{width of minimum cross section}} < 0.5\right)$$

h^*/h_0 has the constant value 2/3 to 1 percent. Only with increasing total heads are the deviations somewhat larger.

38. Water Surface in the Nozzle

a) *Theoretical surface.-* Figure 77a shows the computed disturbance lines for the half-nozzle. Since the side walls of 3-millimeter-thick sheet brass showed small deviations with respect to the nozzle drawn in figure 34 (straight line QR, circle RS, and portion determined by them ST), the actual wall in figure 77a and the corresponding boundary layer were laid as a basis for the determination of the flow by the characteristics method. In order to obtain the lines of constant water depth with sufficient accuracy, the velocity deflection was chosen in steps of $1/2°$.

On figure 77b are drawn the lines of constant water
depth and also the measured depth contours for the total
head h_o = 31.1 mm.

b) Measured water surfaces.- For six different total
heads the water surface was obtained with the apparatus de-
scribed in section 29. In each measurement the flow was
sufficiently stationary. By polishing and cleaning the
side walls a condition was obtained where hardly any capil-
lary waves on the water surface appeared except for some
waves toward the nozzle exit.

Figures 78a-f show the test results. All depth data
refer to a point in the minimum cross section 0.5 mm above
the bottom. Since the thickness of the boundary layer for
the flow with h_o = 80 mm is δ_v = 0.5 mm, the depth
measurements for this total head is directly comparable
with the theory. In the other measurements, corrections
were to be made for h of from +0.05 mm for h_o = 100 mm
to -0.25 mm for h_o = 25 mm, depending on the total head
and the corresponding thickness, according to figure 71.

The symmetry of the depth contours to the nozzle axis
is well satisfied. From these measurements (figs. 78a-f)
the water-depth ratio h/h_o along the nozzle axis was ob-
tained and compared with the theoretical (fig. 79).

39. Comparison of Measurements with Theory and Conclusions

Figure 77b shows that for the total head h_o = 31.1 mm,
there is satisfactory agreement between theory and experi-
ment both with regard to the depth curves and the magnitude
of the depths.

For the large total heads, 100, 80, and 60 mm, there
is, however, a deviation that is not to be overlooked.
The water surfaces for these heads have, in the lower por-
tion of the nozzle, a well-marked valley (figs. 78a,b,c),
with an adjoining hill while, according to the theory of
the two-dimensional flow of shooting water, the surface in
that region should be horizontal. Also, the character of
the depth contours deviates from the theoretical for the
large heads. In the first place, the two side valleys
move too slowly upstream toward the center of the channel
and reach the latter too late. Secondly, they have in the
theoretically straight portion a break which becomes more
marked toward the nozzle end.

With decreasing total head, $h_o = 60, 40, 30$ mm, the depth contours show more nearly the theoretical appearance and the water-depth ratios also agree in magnitude. Figure 79 shows very clearly how, with decreasing water depth, the appearance of the surface along the nozzle axis tends more toward the theoretical and, for $h_o = 40, 30,$ and 25 mm, almost agrees with it.

Only for still smaller total heads do the deviations again increase on account of the decreasing measuring accuracy and on account of the relatively increasing effect of the bottom boundary layer.

The reason for the increasing deviation with increasing water depth is probably to be found in the fact that the assumption of the theory - namely, the neglecting of dw/dt, compared with the acceleration of gravity, is no longer quite satisfied.*

It may further be seen from figure 79 that at the minimum cross section for all total heads, there is a deviation which does not decrease with decreasing water depth. This is the interaction discussed in sections 32 and 33, of the boundary layer with the flow at the critical positions.

As long as the assumptions of the theory are satisfied, the stationary flow of shooting water with free surface may be determined by the characteristics method. It is here a question of determining the first approximation of the three-dimensional flow of an incompressible fluid, and this may be computed as a two-dimensional flow of a compressible fluid.

40. Photographs

In the following, a collection of several flow photographs is presented. Figure 80 shows for a large total head h_o that the water flows through the nozzle with approximately parallel flow at the exit. The capillary waves are here desirable since the waves reflected by them allow the shape of the water surface to be seen.

---

*An estimate of the order of magnitude gives for the Laval nozzle investigated

$$\frac{dw/dt}{g} = \frac{u\frac{\partial w}{\partial x} + v\frac{\partial w}{\partial y} + w\frac{\partial w}{\partial z}}{g} = 0.04 \quad \text{for} \quad h_o = 100 \text{ mm} \quad \text{and}$$

$$0.003 \quad " \quad h_o = 30 \text{ mm}$$

Figures 81a-h show the flow at the nozzle exit for constant total head h_0 but decreasing water depth of the lower water into which the nozzle empties. Figure 81a shows the right hydraulic jump. If the lower water is banked still higher, this jump travels upstream into the nozzle and loses its normal front in the interior where the flow is no longer parallel. In figure 81c the lower water level is still higher than the water depth at the nozzle exit. The two slant hydraulic jumps that arise, cross each other. In figure 81d, the two jet boundaries are almost parallel, while in figures 81e-h, the lower water level lies lower than the surface at the nozzle end and for this reason there occurs a sinking at the edge and the jet "explodes." The end of the sinking - the darker lines starting from the edges which are at the same time the inner boundaries of the light reflections - may be clearly distinguished from the jet boundary, which is approximately given by the outer boundary of the light reflections on the water.

Figure 82a shows a cylindrical body which has somewhat the shape of a cutwater in the parallel flow with $M = 2$. Figure 82b shows the same body from behind, viewed obliquely. Comparison of this picture with figure 83 (reference 5) shows to a surprising degree the analogy of the compressible gas flow with the water flow with free upper surface. In particular, there should also be noted the region behind the body.

The same tapered body produces, when set obliquely to the flow and the deflecting angle of the flow is greater than the critical shock angle corresponding to the approach velocity, a quite different flow (fig. 84). The shock no longer lies at the edge and the shock wave front is no longer straight, but bent.

Figure 85 shows another cutwater-shaped body whose taper half-angle is greater than the critical angle of the approach flow. The shock separates from the edge and would travel upstream to infinity if the sides deflecting the stream were infinitely long. Only because the body has a finite length does the shock-wave front remain stationary at a finite distance ahead of the body. The shock, however, has changed its character as compared with that for the more tapered body. The front is curved and only at some distance does it pass over into the form of shock obtained with the other body. With both flows (figs. 82 and

95) the shock decreases in intensity with increasing dis-
tance from the body similarly on account of the finite size
of the body.

REFERENCES

1. Lamb, H.: Lehrbuch der Hydrodynamik. Deutsche Aus-
      gabe, zweite Auflage, 1931, S. 307-308. G. B.
      Teubner, Leipzig und Berlin.

2. Meyer, Th.: Über zweidimensionale Bewegungsvorgänge
      in einem Gas, das mit Überschallgeschwindigkeit
      strömt. Mitteilungen über Forschungsarbeiten auf
      dem Gebiete des Ing.-Wesens, Heft 62, Berlin, 1908,
      Abschnitt b), S. 46-57. (Dissert. Göttingen.)

    Busemann, A.: Gasdynamik. Handbuch der Experimental-
      physik, Bd. 4, sec. 27, 1931, S. 431-440. Akadem-
      ische Verlagsgesellschaft, Leipzig.

3. Prandtl, L., and Busemann, A.: Näherungsverfahren zur
      zeichnerischen Ermittlung von ebenen Strömungen mit
      Überschallgeschwindigkeit. Festschrift Dr. A.
      Stodola. Orell-Fussli, Zürich, 1929, S. 502.

    Busemann, A.: (See reference 2, S. 374 and 439.)

4. von Kármán, Th.: Eine praktische Anwendung der Analo-
      gie zwischen Überschall-Strömung in Gasen und über-
      kritischer Strömung in offenen Gerinnen. Z.f.a.M.M.,
      Bd. 18, Nr. 1, 1938.

5. Ackeret, J.: Gasdynamik. Handbuch der Physik, Bd. 8,
      1925, S. 338, Abb. 61. Herausgeber Geiger und Scheel,
      Springer.

List of Most Frequently Occurring Symbols

g,   acceleration of gravity.

R,   gas constant.

υ,   kinematic viscosity.

ρ,   density.

p,   pressure.

T,   absolute temperature.

i,   heat content.

c_p,   specific heat at constant pressure.

c_v,   specific heat at constant volume.

$k = c_p/c_v$,   adiabatic exponent.

Φ,   velocity potential.

X,   position-determining potential.

x,y,z,   rectangular coordinates in the flow space.

r,ϑ,   polar coordinates in the flow plane (x,y).

λ,μ,   curvilinear coordinates in the velocity plane,
                characteristic coordinates.

X,Y,Z,   general variables.

u,v,w,   components of the velocity in the x,y, and z.
                directions.

c,φ,   polar coordinates in the velocity diagram (two-
                dimensional flow).

c_{max},   maximum velocity.

Δc,   velocity increment.

a,   in gas: velocity of sound.
            in water: propagation-wave velocity $\sqrt{gh}$.

a^*,   critical velocity.

$\bar{u}, \bar{v}, \bar{c}, \ldots$, nondimensional velocities (reference velocity a^*; in hydraulic jump a^*_1 the critical velocity before the jump).

$M = c/a$, Mach number.

$\alpha = (\sin^{-1})(a/c)$, Mach angle.

h, water depth.

h_0, total head (water depth for $c = 0$).

h_0', h_0'', total heads after hydraulic jumps.

p_0, T_0, i_0, h_0, subscript 0: stagnation state.

$T^*, h^*, \ldots$, asterisk * : critical state.

u_1, c_1, h_1, M_1, subscript 1: before hydraulic jump.

u_2, c_2, h_2, M_2, subscript 2: after hydraulic jump.

u_{2g}, velocity after right hydraulic jump.

$A(X, Y), B, C$, coefficients of linear partial differential equation of second order.

a, b, c, coefficients of the differential equation in normal form.

K, coefficient of the differential equation of the flow in normal form.

δ, small deflection angle.

ω, deflection angle of the flow without dissipation.

β, deflection angle for hydraulic jump.

γ, angle of the hydraulic jump wave front.

Section 31: δ,   boundary-layer thickness.

α, β, γ,   constants of the affine velocity profiles.

(fig. 71) $\left\{ \begin{array}{l} \delta_V = \alpha\,\delta, \text{ volume boundary-layer thickness.} \\ \delta_i = \beta\,\delta, \text{ momentum boundary-layer thickness.} \\ \delta_T = \gamma\,\delta, \text{ tangent intercept.} \end{array} \right.$

TABLE II

Water, k = 2

$\omega = \dfrac{\lambda+\mu}{2}$ (deg.)	$\dfrac{h}{h_0}$	$\bar{c} = \dfrac{c}{a^*}$	$M = \dfrac{c}{a}$	K	$\omega = \dfrac{\lambda+\mu}{2}$ (deg.)	$\dfrac{h}{h_0}$	$\bar{c} = \dfrac{c}{a^*}$	$M = \dfrac{c}{a}$	K
0	2/3	1.000	1.000	∞	26	0.234	1.516	2.56	−0.160
1	0.624	1.062	1.098	2.68	27	.223	1.527	2.64	−.177
2	.598	1.101	1.160	2.07	28	.212	1.538	2.73	−.196
3	.576	1.129	1.214	1.40	29	.201	1.549	2.82	−.216
4	.555	1.156	1.267	1.014	30	.190	1.559	2.92	−.234
5	.535	1.182	1.319	.758	31	.180	1.569	3.02	−.252
6	.516	1.207	1.371	.590	32	.170	1.579	3.13	−.271
7	.498	1.229	1.422	.476	33	.160	1.588	3.24	−.291
8	.481	1.249	1.470	.394	34	.151	1.597	3.36	−.313
9	.464	1.269	1.520	.318	35	.141	1.605	3.49	−.336
10	.448	1.288	1.570	.263	36	.132	1.613	3.63	−.36
11	.432	1.306	1.622	.215	37	.123	1.621	3.78	−.38
12	.417	1.323	1.674	.170	38	.115	1.629	3.93	−.40
13	.402	1.340	1.727	.133	39	.107	1.637	4.01	−.43
14	.387	1.356	1.781	.103	40	.099	1.644	4.26	−.46
15	.373	1.372	1.835	.072	41	.092	1.651	4.44	−.49
16	.359	1.387	1.89	.046	42	.085	1.657	4.63	−.52
17	.345	1.402	1.95	.020	43	.078	1.663	4.85	−.54
18	.331	1.416	2.01	−.004	44	.072	1.669	5.08	−.58
19	.318	1.430	2.07	−.028	45	.066	1.675	5.33	−.62
20	.305	1.444	2.13	−.050	46	.060	1.681	5.62	−.66
21	.292	1.457	2.20	−.071	47	.054	1.686	5.95	−.70
22	.280	1.470	2.27	−.089	48	.048	1.691	6.30	−.75
23	.268	1.482	2.34	−.108	49	.043	1.696	6.68	−.81
24	.256	1.494	2.41	−.126	50	.038	1.700	7.11	−.86
25	.245	1.505	2.48	−.143	65° 53'	0	$\sqrt{3}$	∞	→∞

(For table I, see Part I, T.M. No. 934)

TABLE III

$$d\omega/d\,(h/h_0) = \sqrt{3}\ \sqrt{2/3 - h/h_0}/2\,(1 - h/h_0)\,\sqrt{h/h_0} \qquad (100)$$

h/h_0	$d\omega/d(h/h_0)$	$d(h/h_0)/d\omega$
2/3	0	∞
0.65	22.7°/1	0.0441/o
.625	34.2°/1	.0292/o
.60	41.4	.0242
.575	46.6	.0214
.55	50.8	.0197
.525	54.2	.0184
.5	57.4	.0174
.45	62.7	.0159
.4	67.6	.0148
.35	72.7	.01375
.3	78.4	.01276
.25	85.6	.01168
.2	94.8	.01054
.15	108	.00923
.1	131	.00762
.07	156	.00642
0	∞	0

TABLE IV

Normal Hydraulic Jump

$\bar{u}_1$	M_1	h_1/h_0	$\bar{u}_{2g}$	h_2/h_0	h_0'/h_0	$\bar{u}_1 \bar{u}_{2g}$
1.0	1.0	0.667	1.0	0.667	1.0	1.000
1.02	1.032	.653	.980	.679	1.000	1.000
1.04	1.063	.639	.960	.692	.999	.999
1.06	1.093	.625	.941	.704	.999	.997
1.08	1.127	.611	.922	.715	.998	.995
1.10	1.161	.597	.903	.726	.998	.993
1.12	1.198	.582	.884	.737	.997	.990
1.14	1.237	.567	.865	.747	.996	.986
1.16	1.276	.552	.846	.756	.994	.981
1.18	1.318	.536	.827	.765	.993	.976
1.20	1.359	.520	.808	.772	.990	.970
1.22	1.404	.504	.789	.779	.987	.963
1.24	1.448	.487	.770	.785	.983	.955
1.26	1.498	.472	.751	.791	.979	.946
1.28	1.550	.454	.731	.795	.973	.936
1.30	1.608	.437	.712	.798	.967	.925
1.32	1.667	.419	.692	.799	.959	.914
1.34	1.730	.401	.672	.800	.951	.901
1.36	1.796	.383	.652	.799	.941	.887
1.38	1.867	.366	.632	.798	.931	.872
1.40	1.942	.347	.611	.795	.919	.855
1.45	2.164	.300	.557	.778	.881	.808
1.50	2.45	.250	.500	.751	.834	.750
1.55	2.84	.199	.438	.706	.770	.679
1.60	3.41	.147	.368	.640	.685	.589
1.65	4.43	.092	.285	.542	.566	.470
1.70	7.25	.036	.174	.36	.369	.296
$\sqrt{3}$	∞	0	0	0	0	0

Before jump: h_0,   total head

$\bar{u}_1$,   velocity referred to a^*_1

a^*_1,   critical velocity

M_1,   Mach number

h_1,   water depth

After jump: h_0',   total head

u_{2g},   velocity referred to a^*_1

h_2,   water depth
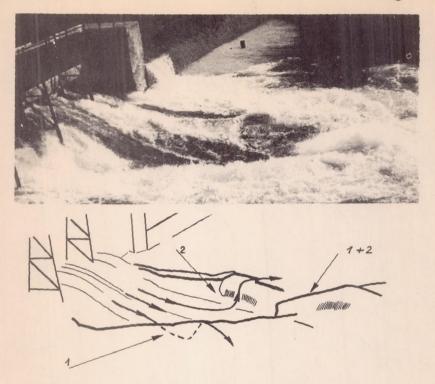
Figure 36.- Slant hydraulic jump.

Figure 35.- Right (orthogonal) hydraulic jump.
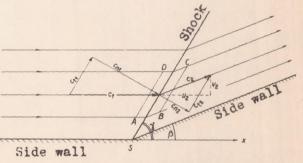
Figure 37.- Slant hydraulic jump (ground plan).
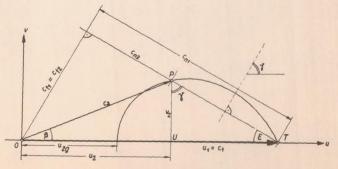
Figure 38.- Hydraulic jump in velocity diagram. Shock polar.
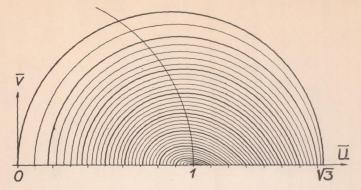
Figure 39.– Shock polar diagram for water.
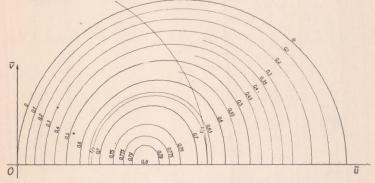
Figure 45.– Lines of constant water depth after the jump.
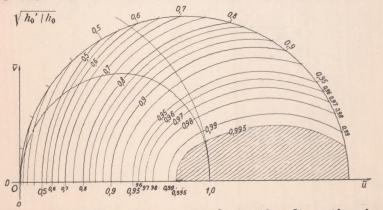
Figure 46.– Lines of constant total depth after the jump.
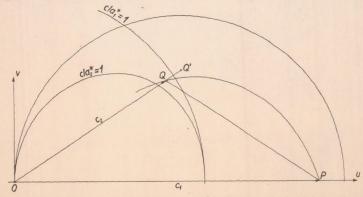
Figure 47.– Boundary line between streaming and shooting after the jump.
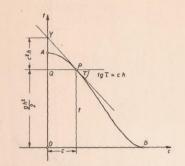
Figure 40.- t, c-curve.
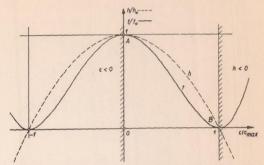
Figure 41.- Character of the t, c-curve ($c^2_{max}=2gh_0$. $t_0=gh_0^2/2$).
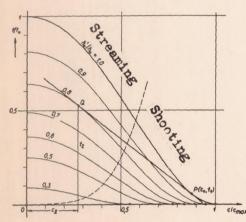
Figure 42.- Right hydraulic jump in t,c-diagram.

$$c^2_{max_0}=2gh_0$$
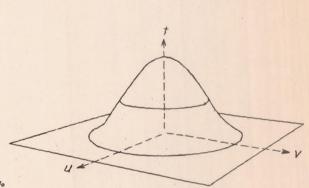
Figure 43.- t-hill.
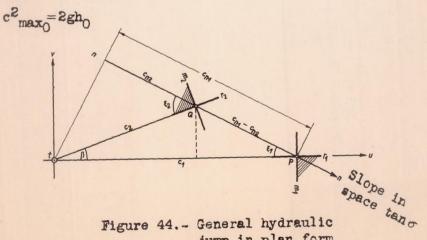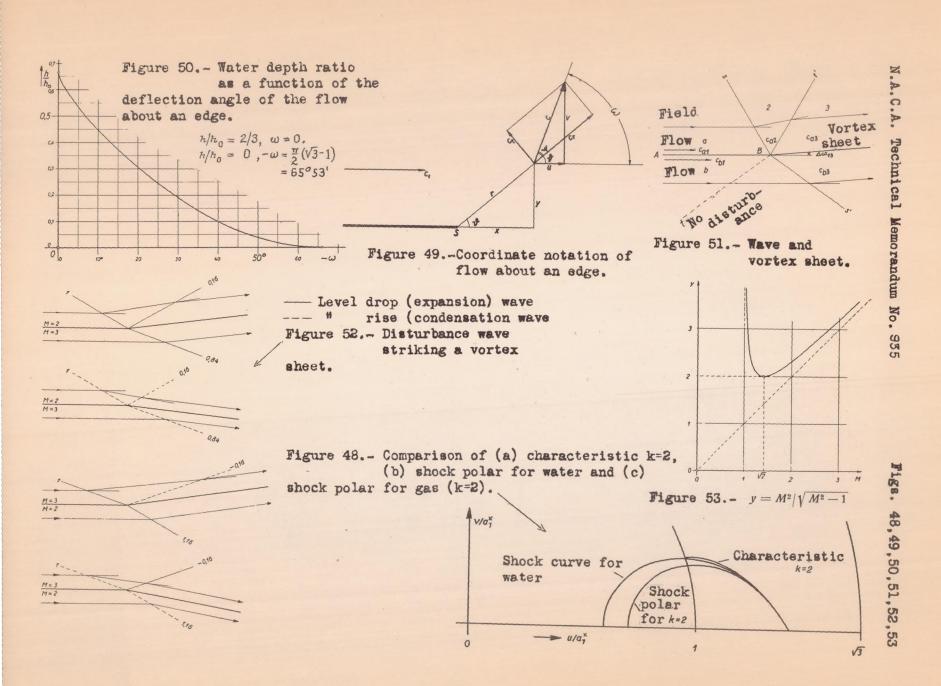
Figure 44.- General hydraulic jump in plan form (see fig. 38).

Figure 50.- Water depth ratio
as a function of the
deflection angle of the flow
about an edge.

$$h/h_0 = 2/3, \quad \omega = 0,$$
$$h/h_0 = 0, \quad -\omega = \frac{\pi}{2}(\sqrt{3}-1)$$
$$= 65°53'$$

Figure 49.- Coordinate notation of
flow about an edge.

Figure 51.- Wave and
vortex sheet.

—— Level drop (expansion) wave
---- " rise (condensation wave

Figure 52.- Disturbance wave
striking a vortex
sheet.

Figure 48.- Comparison of (a) characteristic k=2,
(b) shock polar for water and (c)
shock polar for gas (k=2).

Figure 53.- $y = M^2/\sqrt{M^2-1}$

Shock curve for
water

Characteristic
k=2

Shock
polar
for k=2

Figure 54.- Refraction and reflection of
waves at a vortex sheet.
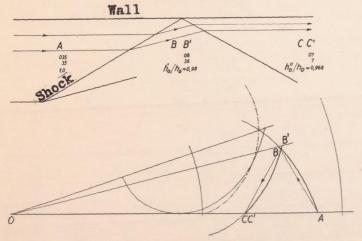
Figure 55.- Reflection of a
hydraulic jump
against a fixed wall.
————Limiting curve.
$h_0''/h_0 = h_0''/h_0' h_0'/h_0$.
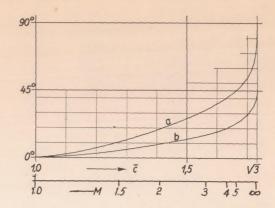
Figure 56.- Critical jump angle
as a function of the
flow of approach.
(a) Simple jump.
(b) Jump reflection (for water).
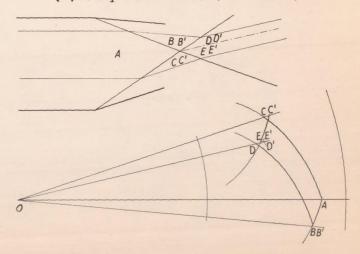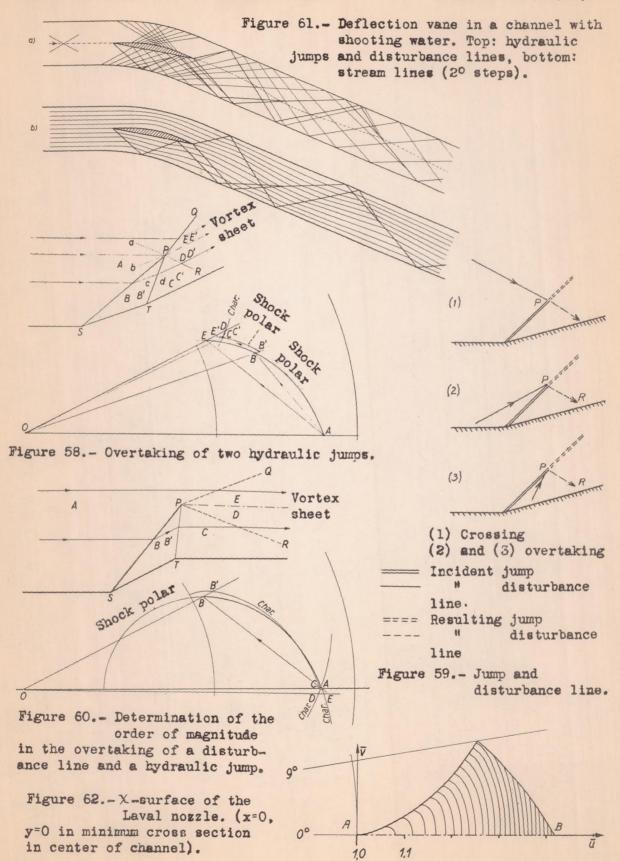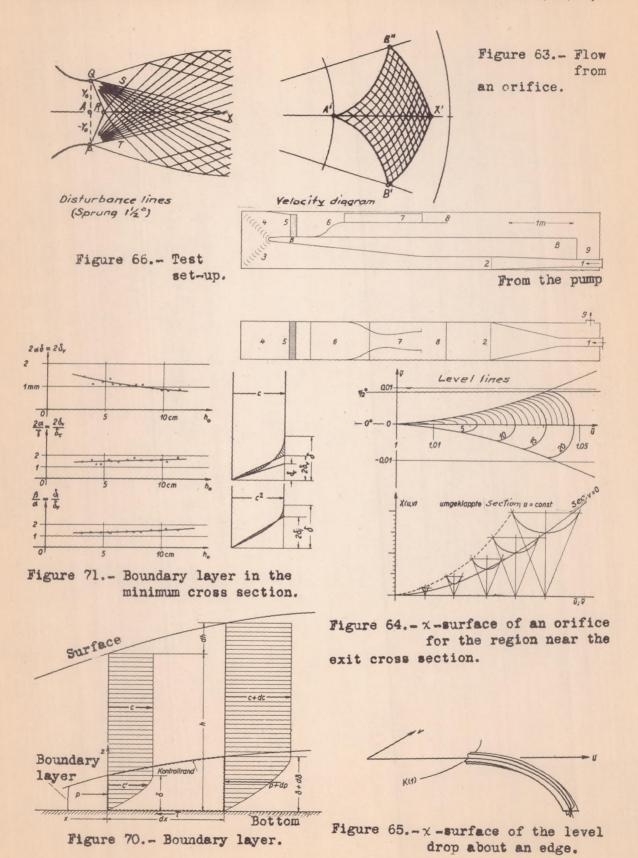
Figure 57.- Crossing of two jumps. (In this
figure D' and E' are drawn sep-
arated though D' practically coincides with E').

Figure 61.- Deflection vane in a channel with shooting water. Top: hydraulic jumps and disturbance lines, bottom: stream lines (2° steps).

Figure 58.- Overtaking of two hydraulic jumps.

(1) Crossing
(2) and (3) overtaking

≣≣≣	Incident jump
"	disturbance line.
====	Resulting jump
----	" disturbance line

Figure 59.- Jump and disturbance line.

Figure 60.- Determination of the order of magnitude in the overtaking of a disturbance line and a hydraulic jump.

Figure 62.- X-surface of the Laval nozzle. (x=0, y=0 in minimum cross section in center of channel).

Figure 63.- Flow
from
an orifice.

Disturbance lines
(Sprung 1½°)

Velocity diagram

Figure 66.- Test
set-up.

From the pump

Figure 71.- Boundary layer in the
minimum cross section.

Level lines

Figure 64.- x-surface of an orifice
for the region near the
exit cross section.

Surface

Boundary
layer

Figure 70.- Boundary layer.

Figure 65.- x-surface of the level
drop about an edge.

Figure 67.- Test nozzle seen from above.
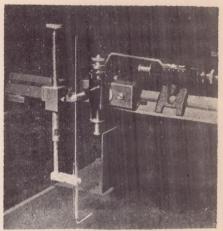
Figure 69.- Boundary layer measurement.

Figure 68.- Test nozzle seen from the nozzle end. Measurement of the water surface.
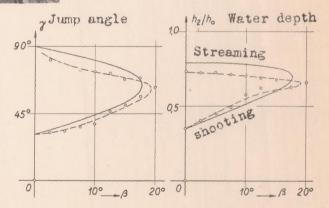
Figure 75.- Hydraulic jump.
——— Theory
——— Experiment
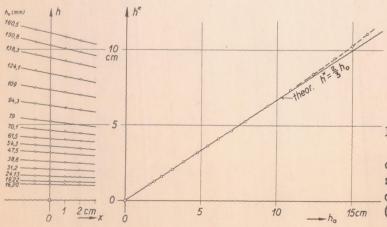
Figure 76.- Water depths in minimum cross section. (a) water surface in the region of minimum cross section (x=0). (b) $h^* = f(h_o)$.

From boundary layer measurement.
"   direct measurement.

Figure 72.- Check the relation
between the boundary
layer thickness and the slope of
the surface from equation (114).

$h_0 = 80$ mm   Equidistance   0,1   und   0,2 mm
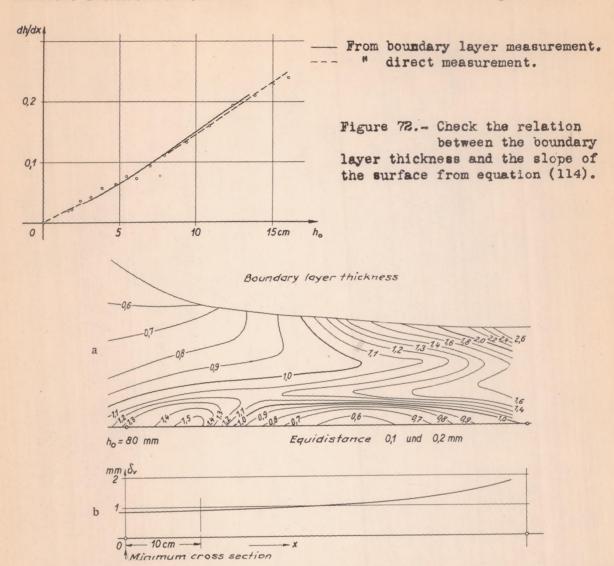
Figure 73.- Side wall boundary layer. (a) total surface, (b) value averaged
over the depth.

$h_0 = 80,5$ mm   Equidistance   0.05   und   0,1 mm
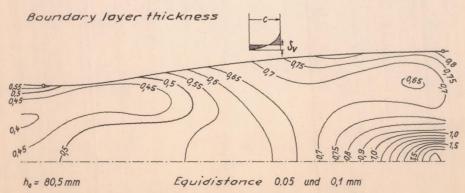
Figure 74.- Bottom boundary layer surface.
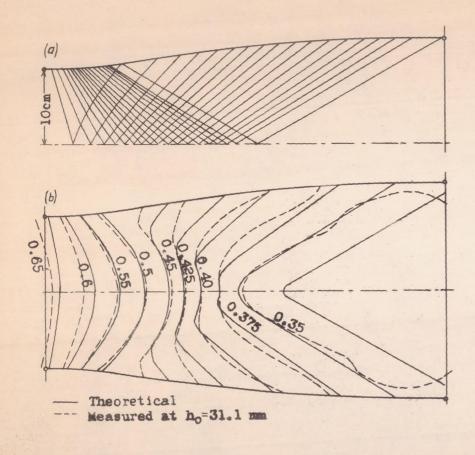
Figure 77.- Actual Laval nozzle. (a) Disturbance
lines (steps 1/2 degree) (b) depth
contours.
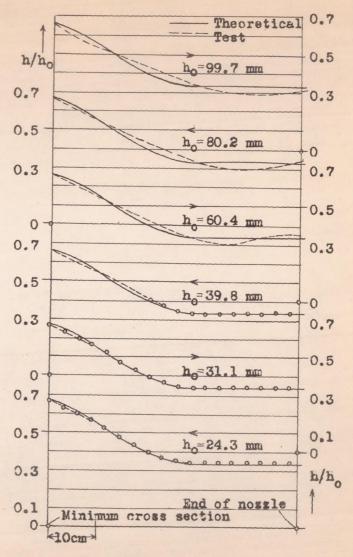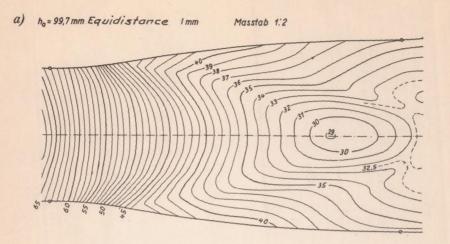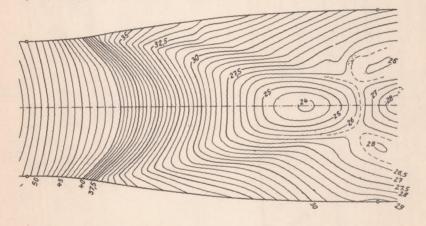
Figure 79.- Water depth ratio along
the nozzle axis.

a) $h_0 = 99.7$ mm Equidistance 1mm   Masstab 1:2

b) $h_0 = 80.2$ mm Equidistance 0.5 und 1 mm

c) $h_0 = 60.4$ mm Equidistance 0.5mm
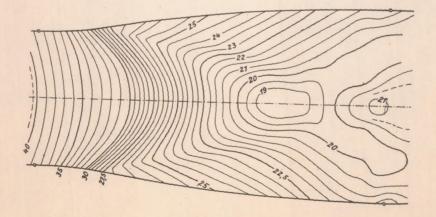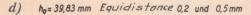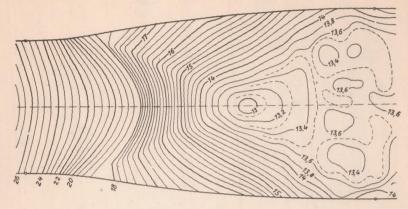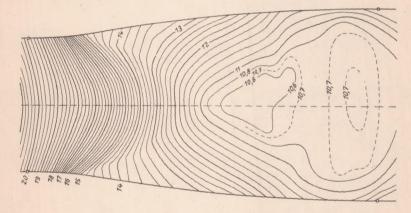
Figure 78a-f.-Measured water surfaces.

d) $h_0 = 39,83$ mm *Equidistance* 0,2 und 0,5mm

e) $h_0 = 31,10$ mm. *Equidistance* 0,2 mm

f) $h_0 = 24,32$ mm *Equidistance* 0,2 mm   Masstab 1:2 Scale
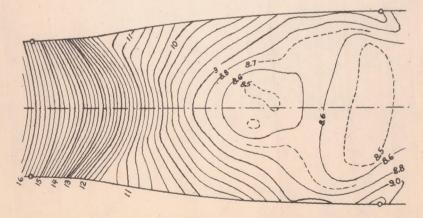
Figure 78a-f.- concluded
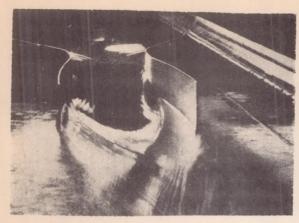
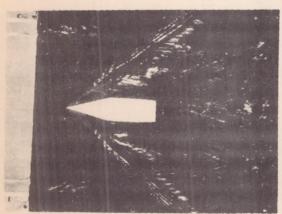Figure 80.- Flow through the nozzle viewed from the nozzle end.
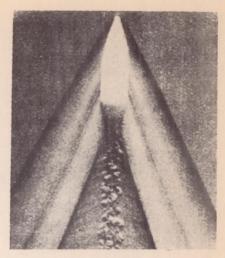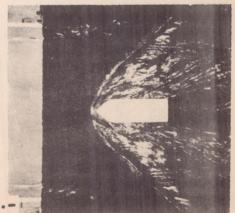

Figure 83.- Bullet in air.

Figure 82a.-

Figure 82b.-

Figure 82.- Tapered body in water. Shock wave starts from the tip.

Figure 84.- Tapered body set obliquely, shock angle above critical.

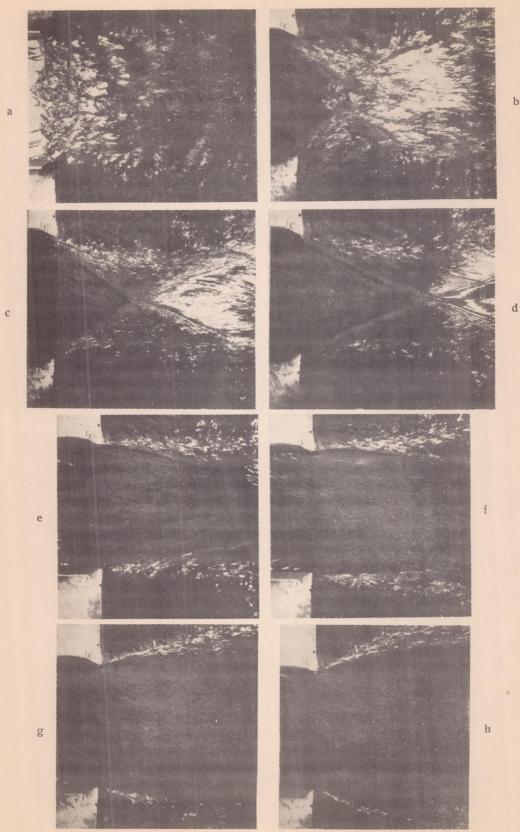Figure 85.- Tapered body whose taper shock angle is greater than the critical angle of the flow; shock wave released by body.

Figure 81a-h.- Various conditions at the nozzle exit.